CHAPTER

9 Constitutive relations and formulation of theories incorporating material microstructure

As mentioned in in Section 6.1, all real materials have internal microstructure at various length scales, and some examples were shown in Figs. 6.1–6.3. Recently, there has been considerable demand on structural performance and this has led to the development of many new heterogeneous synthetic materials with complex microstructures that help provide the desired material properties. Our previous continuum mechanics theories have generally been developed for problems with length scales several orders of magnitude larger than these microstructural features. In this fashion, microstructure is then averaged over these heterogeneous material phases to allow standard continuum mechanics to be employed. We now wish to explore theories that attempt to model some of these microstructural effects by embedding additional features into the classical field equations. Over the last few decades, numerous theories have been developed. Since this is a textbook, we will limit our study and primarily explore several micromechanical continuum theories coupled with linear elasticity. In this fashion, we can easily develop the basic formulations and find a few closed-form micromechanical solutions to compare with corresponding classical predictions. This will provide the reader with some basic micromechanical background on formulation concepts and solution results. Within the elasticity context, we will discuss micropolar, distributed voids, doublet mechanics, higher-gradient theories, fabric tensor models, and some fundamental aspects of damage mechanics.

9.1 INTRODUCTION TO MICROMECHANICS MATERIAL MODELING

In the last several decades, there has been considerable interest in micromechanical modeling of materials. This interest has been motivated by the fact that all real materials and more importantly numerous recent synthetic materials have heterogeneous microstructures that affect the overall load–deformation response. Material heterogeneity occurs at many different length scales, and for continuum mechanics modeling these scales should normally be at least an order or two smaller than the behaviors sought. Based on this, these heterogeneous features are normally referred to as microstructure. Examples of this commonly include atoms, molecules, particulate and

Continuum Mechanics Modeling of Material Behavior. http://dx.doi.org/10.1016/B978-0-12-811474-2.00009-5

fiber composites, soil, rock, concretes, granular materials, porous and cellular solids, and many others.

Micromechanical modeling is often categorized into two general camps that are labeled as *discrete* or *continuum* approaches. Discrete models generally included detailed simulation of the various microstructural phases and geometries, and examples would include atomistic modeling, molecular dynamics, particulate discrete element methods, and many other numerical schemes based on detailed finite-element analysis of specific heterogeneity. Generally, this approach requires extensive numerical and computational effort and is often limited to small length and time scales. On the other hand, continuum micromechanical modeling incorporates additional, continuously distributed fields of various types that bring new features into the theory. These additional relations are then combined with some of the classical equations (kinematics, stress, balance laws) to establish a modified continuum theory. This latter approach will be our focus in this chapter.

One of the fundamental goals of micromechanical material modeling is to develop theories to predict the response of the heterogeneous material on the basis of the geometries and properties of the individual phases. A simple example of this concept is illustrated in Fig. 9.1 which shows a particulate composite material containing particles embedded in a matrix material. The deformation response of this two-phase composite will depend on several features of the material makeup including: particle and matrix material moduli, particular geometries related to particle size and distribution, and bonding between the two phases. The question is: can we develop an *equivalent continuum* that would properly model the composite?

In regard to material behavior, *homogenization* is concerned with developing equivalent continuum theories for materials that contain various heterogeneous microstructural phases and geometries. This is most commonly done by assuming that we can define a statistically equivalent homogeneous medium characterized by a *representative volume element* (RVE) or for ordered microstructure by a *repeating unit cell*

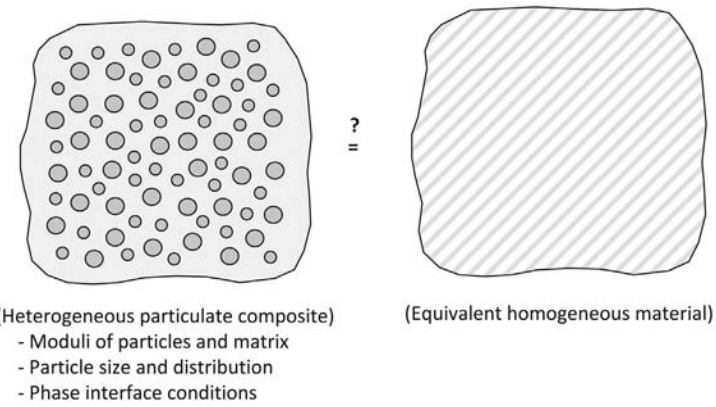

FIGURE 9.1

Heterogeneous particulate composite material.

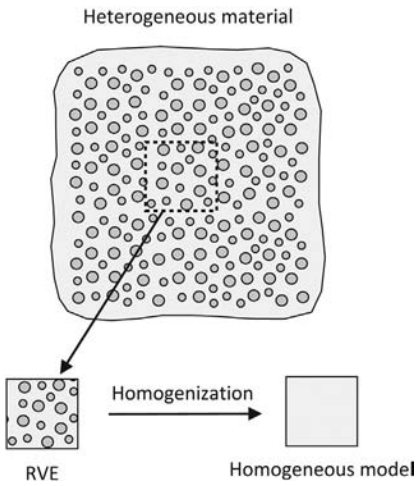

FIGURE 9.2

Concepts of modeling heterogeneous materials.

(RUC). Fig. 9.2 graphically illustrates the basic steps. Hill (1963) was one of the originators of the RVE concept for composite materials. A more general definition of RVE would be that it represents a subvolume of a heterogeneous material by statistically including all microstructural heterogeneities (grains, inclusions, voids, fibers, etc.), thereby creating a homogenized sample. We wish for the RVE to remain small enough to be considered as a volume element in the continuum mechanics sense in order to describe properties at a point. Also, the RVE is expected to properly allow typical prescribed boundary conditions to create mean strain or stress on the material element. Based on microscopic RVE and macroscopic length scales L, we normally need the relation $L_{micro} << L_{RVE} << L_{macro}$ to be satisfied. Once the RVE is determined, a homogenization process is applied to develop the homogeneous model material element. Homogenization is commonly accomplished using either analytical/mathematical methods or numerical/computational schemes. Some of this activity has been described as *meso-mechanical modeling*, that is, being in the middle between micro and macro. Nemat-Nasser and Hori (1993), Charalambakis (2010), Fish and Kuznetsov (2012), and Nguyen et al. (2011) provide reviews and further background on these topics.

Recent analytical studies have constructed various generalizations of classical continuum theories by introducing different kinds of microbehaviors into the basic theory. These models generally go deeply into the basics of continuum mechanics in order to capture these new phenomena. Microbehaviors commonly come from enhanced kinematics, conservation principles, and constitutive relations. Some researchers (Fish and Kuznetsov, 2012) classify these schemes into two categories. One type, sometimes referred to as *higher-order continua*, is characterized by having additional microdegrees of freedom independent of the usual continuum mechanics macro displacements and rotations. The second type of theory may be called *higher*

grade continua and would employ higher-order spatial derivatives of the displacement, thereby generating new types of strain tensors. In the Noll sense (see Section 8.4.2), this type of model becomes a *nonsimple* material. We will pursue examples of each of these cases for linear elastic materials. Geometric material microstructure will commonly introduce *theoretical length scales* into the new models, a feature not found in classical continuum mechanics. As we briefly explore the micromechanical theories, we will look for these new parameters and investigate and compare their effect on problem solution. Ultimately, these theoretical length scales should be somehow connected to length scales associated with the actual material microstructure.

9.2 MICROPOLAR ELASTICITY

The response of many heterogeneous materials has indicated dependency on microscale length parameters such as embedded particle displacement and/or rotation. This would indicate that a continuum model of this material might need additional distributed microstructural degrees of freedom and hence a higher-order continua. Solids exhibiting such behavior include a large variety of cemented particulate materials such as particulate composites, ceramics, and various concretes. This concept can be qualitatively illustrated by considering a simple *lattice model* of a particulate material as shown in Fig. 9.3. Using such a scheme, the macro load transfer within the heterogeneous particulate solid is modeled using the microforces and moments between adjacent particles (see Chang and Ma, 1991; Sadd et al., 1992, 2004). Depending on the microstructural packing geometry (sometimes referred to as *fabric*), this method establishes a lattice network that can be thought of as an interconnect series of elastic bar or beam elements interconnected at particle centers. Thus, the network represents, in some way, the material microstructure and brings microstructural dimensions such as the grid size into the model. Furthermore, the elastic network will establish internal bending moments and forces, which will depend on internal degrees of freedom (e.g. rotations) at each connecting point in the microstructure

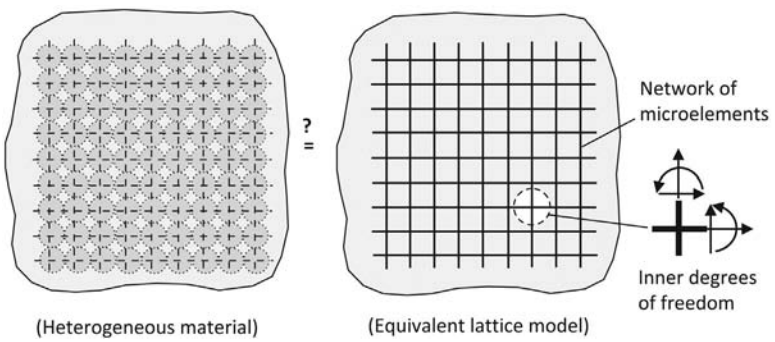

FIGURE 9.3

Heterogeneous material with internal microstructure.

as shown. These internal rotations would be, in a sense, independent of the overall macrodeformations.

This concept then suggests that an elastic continuum theory including an independent rotation field with concentrated pointwise moments might be suitable for modeling such heterogeneous materials. These approaches have been formulated under the names *Cosserat continuum*, *oriented media*, *asymmetric elasticity*, *micropolar*, or *couple-stress theories*. The Cosserat continuum developed in 1909 was historically one of the first models of this category. However, in the next 50 years, very little activity occurred in this field. Renewed interest began during the 1960s, and this produced numerous articles on theoretical refinements and particular analytical and computational applications. Toupin (1964) and Mindlin (1964) developed a general *linear elasticity theory with microstructure* that allowed the stress to depend on both the strain and an additional *kinematic microdeformation* tensor. This and related research has led to the development *couple-stress* and *micropolar theories.* These approaches allow material deformation to include additional independent *microrotational* degrees of freedom. The studies by Eringen (1968) and Kunin (1983) provide detailed background on much of this work, whereas Nowacki (1986) presents a comprehensive account on dynamic and thermoelastic applications of such theories. Later, Eringen (1999) provided additional extensions of the basic micropolar approach. He used the concept of *deformation of material directors* to categorize the microcontinuum into three types: micromorphic with deformable directors, microstretch with directors that only stretch, and micropolar with rigid directors that only rotate. Our study will only include the micropolar case and only for linear elastic materials.

Micropolar theory for linear, elastic small deformation theory incorporates an additional internal degree of freedom called the *microrotation* and allows for the existence *body and surface couples*. For this approach, the new kinematic strain–deformation relation is expressed as

$$\varepsilon_{ij} = u_{j,i} - \varepsilon_{ijl}\phi_l \tag{9.2.1}$$

where ε_{ij} is usual infinitesimal strain tensor, ε_{ijl} is the alternating symbol, u_i is the displacement vector, and ϕ_i is the *microrotation vector*. Note that this new kinematic variable ϕ_i is independent of the displacement u_i and thus is not, in general, the same as the usual macrorotation vector, that is,

$$\omega_i = \frac{1}{2}\varepsilon_{ijk}u_{k,j} \neq \phi_i \tag{9.2.2}$$

Later in our discussion, we will relax this restriction and develop a more specialized theory that normally allows for simpler analytical problem solution.

The existence of body and surface couples (moments) included in the new theory will introduce additional terms in the equilibrium equations. Skipping the derivation details, the linear and angular equilibrium equations thus become

$$\begin{aligned} T_{ji,j} + F_i &= 0 \\ m_{ji,j} + \varepsilon_{ijk}T_{jk} + C_i &= 0 \end{aligned} \tag{9.2.3}$$

where T_{ij} is the usual Cauchy stress tensor, F_i is the body force per unit volume, m_{ij} is the *surface moment tensor* normally referred to as the *couple-stress tensor*, and C_i is the *body couple* per unit volume. Notice that as a consequence of including couple-stresses and body couples, relation $(9.2.3)_2$ implies that *the stress tensor T_{ij} will no longer be symmetric*.

For linear elastic isotropic materials, the constitutive relations for a micropolar material are given by

$$\begin{aligned} T_{ij} &= \lambda\varepsilon_{kk}\delta_{ij} + (\mu+\kappa)\varepsilon_{ij} + \mu\varepsilon_{ji} \\ m_{ij} &= \alpha\phi_{k,k}\delta_{ij} + \beta\phi_{i,j} + \gamma\phi_{j,i} \end{aligned} \tag{9.2.4}$$

where $\lambda, \mu, \kappa, \alpha, \beta, \gamma$ are the micropolar elastic moduli. Note that classical elasticity relations correspond to the case where $\kappa = \alpha = \beta = \gamma = 0$. The requirement of a positive definite strain energy function puts the following restrictions on these moduli:

$$\begin{aligned} &0 \le 3\lambda + 2\mu + \kappa, \quad 0 \le 2\mu + \kappa, \quad 0 \le \kappa \\ &0 \le 3\alpha + \beta + \gamma, \quad -\gamma \le \beta \le \gamma, \quad 0 \le \gamma \end{aligned} \tag{9.2.5}$$

Relations (9.2.1) and (9.2.4) can be substituted into the equilibrium equations (9.2.3) to establish two sets of governing field equations in terms of the displacements and microrotations. Appropriate boundary conditions to accompany these field equations are somewhat more problematic. For example, it is not completely clear as to how to specify the microrotation ϕ_i and/or couple-stress m_{ij} on domain boundaries. Some developments on this subject have determined particular field combinations whose boundary specification guarantees a unique solution to the problem.

Two-dimensional couple-stress theory

Rather than continuing on with the general three-dimensional equations, we will now move directly into two-dimensional problems under plane strain conditions. In addition to the usual assumption $u = u(x,y), v = v(x,y), w = 0$, we include the restrictions on the microrotation, $\phi_x = \phi_y = 0, \phi_z = \phi_z(x,y)$. Furthermore, relation (9.2.2) will be relaxed and *the microrotation will be allowed to coincide with the macrorotation*:

$$\phi_i = \omega_i = \frac{1}{2}\varepsilon_{ijk}u_{k,j} \tag{9.2.6}$$

This particular theory is then a special case of micropolar elasticity and is commonly referred to *couple-stress theory.* Eringen (1968) refers to this theory as *indeterminate* since the antisymmetric part of the stress tensor is not determined solely by the constitutive relations.

Stresses on a typical in-plane element are shown in Fig. 9.4. Notice the similarity of this force system with the microstructural system illustrated previously in Fig. 9.3. For the two-dimensional case with no body forces or body couples, the equilibrium equations (9.2.3) reduce to

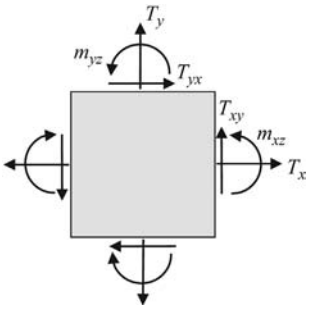

FIGURE 9.4

Couple-stresses on two-dimensional element.

$$\begin{aligned}\frac{\partial T_{xx}}{\partial x}+\frac{\partial T_{yx}}{\partial y}&=0\\ \frac{\partial T_{xy}}{\partial x}+\frac{\partial T_{yy}}{\partial y}&=0\\ \frac{\partial m_{xz}}{\partial x}+\frac{\partial m_{yz}}{\partial y}+T_{xy}-T_{yx}&=0\end{aligned}\tag{9.2.7}$$

The in-plane strains can be expressed as

$$\begin{aligned}\varepsilon_x=\frac{\partial u}{\partial x},\quad \varepsilon_y&=\frac{\partial v}{\partial y}\\ \varepsilon_{xy}=\frac{\partial v}{\partial x}-\phi_z,\quad \varepsilon_{yx}&=\frac{\partial u}{\partial y}+\phi_z\end{aligned}\tag{9.2.8}$$

while using (9.2.6) gives

$$\phi_z=\frac{1}{2}\left(\frac{\partial v}{\partial x}-\frac{\partial u}{\partial y}\right)\tag{9.2.9}$$

Notice that by substituting (9.2.9) into $(9.2.8)_2$ gives the result $\varepsilon_{xy}=\varepsilon_{yx}$.

The constitutive equations (9.2.4) yield the following forms for the stress components:

$$\begin{aligned}T_{xx}&=\lambda(\varepsilon_x+\varepsilon_y)+(2\mu+\kappa)\varepsilon_x\\ T_{yy}&=\lambda(\varepsilon_x+\varepsilon_y)+(2\mu+\kappa)\varepsilon_y\\ T_{xy}&=(2\mu+\kappa)\varepsilon_{xy}=T_{yx}\\ m_{xz}=\gamma\frac{\partial\phi_z}{\partial x},\quad m_{yz}&=\gamma\frac{\partial\phi_z}{\partial y}\end{aligned}\tag{9.2.10}$$

In regard to the last pair of equations in (9.2.10), some authors (Mindlin, 1963; Boresi and Chong, 2000) define the gradients of the rotation ϕ_z as the *curvatures*. Thus, they establish a linear constitutive law between the couple-stresses and curvatures. This approach is completely equivalent to the current method. It is to be noted from (9.2.10) that under the assumptions of couple-stress theory, we find the

unpleasant situation that the antisymmetric part of the stress tensor disappears from the constitutive relations. In order to remedy this, we can solve for the antisymmetric stress term from the moment equilibrium equation $(9.2.7)_3$ to get

$$T_{[xy]} = \frac{1}{2}(T_{xy} - T_{yx}) = -\frac{1}{2}\left(\frac{\partial m_{xz}}{\partial x} + \frac{\partial m_{yz}}{\partial y}\right) = -\frac{\gamma}{2}\nabla^2\phi_z \tag{9.2.11}$$

By cross-differentiation, we can eliminate the displacements from (9.2.8) and (9.2.9) and develop the particular compatibility equations for this case

$$\begin{gathered}
\frac{\partial^2 \varepsilon_x}{\partial y^2} + \frac{\partial^2 \varepsilon_y}{\partial x^2} = 2\frac{\partial^2 \varepsilon_{xy}}{\partial x \partial y} \\
\frac{\partial^2 \phi_z}{\partial x \partial y} = \frac{\partial^2 \phi_z}{\partial y \partial x} \\
\frac{\partial \phi_z}{\partial x} = \frac{\partial \varepsilon_{xy}}{\partial x} - \frac{\partial \varepsilon_x}{\partial y} \\
\frac{\partial \phi_z}{\partial y} = \frac{\partial \varepsilon_y}{\partial x} - \frac{\partial \varepsilon_{xy}}{\partial y}
\end{gathered} \tag{9.2.12}$$

Using the constitutive forms (9.2.10), these relations may be expressed in terms of the stresses as

$$\begin{gathered}
\frac{\partial^2 T_{xx}}{\partial y^2} + \frac{\partial^2 T_{yy}}{\partial x^2} - \nu\nabla^2(T_{xx} + T_{yy}) = \frac{\partial^2}{\partial x \partial y}(T_{xy} + T_{yx}) \\
\frac{\partial m_{xz}}{\partial y} = \frac{\partial m_{yz}}{\partial x} \\
m_{xz} = l^2 \frac{\partial}{\partial x}(T_{xy} + T_{yx}) - 2l^2 \frac{\partial}{\partial y}[T_{xx} - \nu(T_{xx} + T_{yy})] \\
m_{yz} = 2l^2 \frac{\partial}{\partial x}[T_{yy} - \nu(T_{xx} + T_{yy})] - l^2 \frac{\partial}{\partial y}(T_{xy} + T_{yx})
\end{gathered} \tag{9.2.13}$$

where $\nu = \lambda/(2\lambda + 2\mu + \kappa)$, and $l = \sqrt{\gamma/(4\mu + 2\kappa)}$ is a material constant with units of *length*. Notice that this result then introduces a *length scale* into the problem. If $l = 0$, the couple-stress effects are eliminated and the problem reduces to classical elasticity. It should also be pointed out that only three of the four equations in set (9.2.13) are independent as the second relation can be established from the other equations.

Proceeding along similar lines as classical elasticity, we introduce a stress function approach Carlson (1966) to solve (9.2.13). A self-equilibrated form satisfying (9.2.7) identically can be written as

$$\begin{gathered}
T_{xx} = \frac{\partial^2 \Phi}{\partial y^2} - \frac{\partial^2 \Psi}{\partial x \partial y}, \quad T_{yy} = \frac{\partial^2 \Phi}{\partial x^2} + \frac{\partial^2 \Psi}{\partial x \partial y} \\
T_{xy} = -\frac{\partial^2 \Phi}{\partial x \partial y} - \frac{\partial^2 \Psi}{\partial y^2}, \quad T_{yx} = -\frac{\partial^2 \Phi}{\partial x \partial y} + \frac{\partial^2 \Psi}{\partial x^2} \\
m_{xz} = \frac{\partial \Psi}{\partial x}, \quad m_{yz} = \frac{\partial \Psi}{\partial y}
\end{gathered} \tag{9.2.14}$$

where $\Phi = \Phi(x, y)$ and $\Psi = \Psi(x, y)$ are the stress functions for this case. If Ψ is taken to be zero, the representation reduces to the usual Airy form (6.2.47) with no couple-stresses. Using form (9.2.14) in the compatibility equations (9.2.13) produces

$$\begin{aligned} \nabla^4\Phi &= 0 \\ \frac{\partial}{\partial x}(\Psi - l^2\nabla^2\Psi) &= -2(1-\nu)l^2\frac{\partial}{\partial y}(\nabla^2\Phi) \\ \frac{\partial}{\partial y}(\Psi - l^2\nabla^2\Psi) &= 2(1-\nu)l^2\frac{\partial}{\partial x}(\nabla^2\Phi) \end{aligned} \tag{9.2.15}$$

Differentiating the second equation with respect to x and the third with respect to y and adding will eliminate the Φ function and give the following result:

$$\nabla^2\Psi - l^2\nabla^4\Psi = 0 \tag{9.2.16}$$

Thus, the two stress functions satisfy governing equations $(9.2.15)_1$ and (9.2.16). We will now consider a specific application of this theory for the following stress concentration problem.

EXAMPLE 9.2.1 MICROPOLAR ELASTICITY STRESS CONCENTRATION AROUND A CIRCULAR HOLE UNDER UNIFORM UNIAXIAL LOADING

We now wish to investigate the effects of couple-stress theory on the two-dimensional stress distribution around a circular hole in an infinite medium under uniform tension T at infinity. Recall that this problem was previously solved for the nonpolar case in Example 6.2.4 and the problem geometry is shown in Fig. 6.12. The hole is to have radius a, and the far-field stress is directed along the x-direction as shown. The solution for this case will be first developed for the micropolar model and then the additional simplification for couple-stress theory will be incorporated. This solution was first presented by Kaloni and Ariman (1967) and later by Eringen (1968).

Solution: As expected, for this problem, the plane strain formulation and solution is best done in polar coordinates. For this system, the equilibrium equations become

$$\begin{aligned} \frac{\partial T_{rr}}{\partial r} + \frac{1}{r}\frac{\partial T_{\theta r}}{\partial \theta} + \frac{T_{rr} - T_{\theta\theta}}{r} &= 0 \\ \frac{\partial T_{r\theta}}{\partial r} + \frac{1}{r}\frac{\partial T_{\theta\theta}}{\partial \theta} + \frac{T_{r\theta} - T_{\theta r}}{r} &= 0 \\ \frac{\partial m_{rz}}{\partial r} + \frac{1}{r}\frac{\partial m_{\theta z}}{\partial \theta} + \frac{m_{rz}}{r} + T_{r\theta} - T_{\theta r} &= 0 \end{aligned} \tag{9.2.17}$$

while the strain–deformation relations are

$$\begin{aligned}
\varepsilon_r &= \frac{\partial u_r}{\partial r}, \quad \varepsilon_\theta = \frac{1}{r}\left(\frac{\partial u_\theta}{\partial \theta} + u_r\right) \\
\varepsilon_{r\theta} &= \frac{\partial u_\theta}{\partial r} - \phi_z, \quad \varepsilon_{\theta r} = \frac{1}{r}\left(\frac{\partial u_r}{\partial \theta} - u_\theta\right) + \phi_z
\end{aligned} \tag{9.2.18}$$

The constitutive equations in polar coordinates read as

$$\begin{aligned}
T_{rr} &= \lambda(\varepsilon_r + \varepsilon_\theta) + (2\mu + \kappa)\varepsilon_r \\
T_{\theta\theta} &= \lambda(\varepsilon_r + \varepsilon_\theta) + (2\mu + \kappa)\varepsilon_\theta \\
T_{r\theta} &= (\mu + \kappa)\varepsilon_{r\theta} + \mu\varepsilon_{\theta r}, \quad T_{\theta r} = (\mu + \kappa)\varepsilon_{\theta r} + \mu\varepsilon_{r\theta} \\
m_{rz} &= \gamma\frac{\partial \phi_z}{\partial r}, \quad m_{\theta z} = \gamma\frac{1}{r}\frac{\partial \phi_z}{\partial \theta}
\end{aligned} \tag{9.2.19}$$

and the strain–compatibility relations take the form

$$\begin{aligned}
\frac{\partial \varepsilon_{\theta r}}{\partial r} - \frac{1}{r}\frac{\partial \varepsilon_r}{\partial \theta} + \frac{\varepsilon_{\theta r} - \varepsilon_{r\theta}}{r} - \frac{\partial \phi_z}{\partial r} &= 0 \\
\frac{\partial \varepsilon_\theta}{\partial r} - \frac{1}{r}\frac{\partial \varepsilon_{r\theta}}{\partial \theta} + \frac{\varepsilon_\theta - \varepsilon_r}{r} - \frac{1}{r}\frac{\partial \phi_z}{\partial \theta} &= 0 \\
\frac{\partial m_{\theta z}}{\partial r} - \frac{1}{r}\frac{\partial m_{rz}}{\partial \theta} + \frac{m_{\theta z}}{r} &= 0
\end{aligned} \tag{9.2.20}$$

For the polar coordinate case, the stress–stress function relations become

$$\begin{aligned}
T_{rr} &= \frac{1}{r}\frac{\partial \Phi}{\partial r} + \frac{1}{r^2}\frac{\partial^2 \Phi}{\partial \theta^2} - \frac{1}{r}\frac{\partial^2 \Psi}{\partial r \partial \theta} + \frac{1}{r^2}\frac{\partial \Psi}{\partial \theta} \\
T_{\theta\theta} &= \frac{1}{r^2}\frac{\partial^2 \Phi}{\partial r^2} + \frac{1}{r}\frac{\partial^2 \Psi}{\partial r \partial \theta} - \frac{1}{r^2}\frac{\partial \Psi}{\partial \theta} \\
T_{r\theta} &= -\frac{1}{r}\frac{\partial^2 \Phi}{\partial r \partial \theta} + \frac{1}{r^2}\frac{\partial \Phi}{\partial \theta} - \frac{1}{r}\frac{\partial \Psi}{\partial r} - \frac{1}{r^2}\frac{\partial^2 \Psi}{\partial \theta^2} \\
T_{\theta r} &= -\frac{1}{r}\frac{\partial^2 \Phi}{\partial r \partial \theta} + \frac{1}{r^2}\frac{\partial \Phi}{\partial \theta} + \frac{\partial^2 \Psi}{\partial r^2} \\
m_{rz} &= \frac{\partial \Psi}{\partial r}, \quad m_{\theta z} = \frac{1}{r}\frac{\partial \Psi}{\partial \theta}
\end{aligned} \tag{9.2.21}$$

Using constitutive relations (9.2.19), the compatibility equations (9.2.20) can be expressed in terms of stresses, and combining this result with (9.2.21) will yield the governing equations for the stress functions in polar coordinates:

$$\begin{aligned}
\frac{\partial}{\partial r}(\Psi - l_1^2 \nabla^2 \Psi) &= -2(1 - \nu) l_2^2 \frac{1}{r}\frac{\partial}{\partial \theta}(\nabla^2 \Phi) \\
\frac{1}{r}\frac{\partial}{\partial \theta}(\Psi - l_1^2 \nabla^2 \Psi) &= 2(1 - \nu) l_2^2 \frac{\partial}{\partial r}(\nabla^2 \Phi)
\end{aligned} \tag{9.2.22}$$

where

$$l_1^2 = \frac{\gamma(\mu+\kappa)}{\kappa(2\mu+\kappa)}, \quad l_2^2 = \frac{\gamma}{2(2\mu+\kappa)}$$
$$\nabla^2 = \frac{\partial^r}{\partial r^2} + \frac{1}{r}\frac{\partial}{\partial r} + \frac{1}{r^2}\frac{\partial^2}{\partial \theta^2} \tag{9.2.23}$$

Note that for the micropolar case, *two length parameters* l_1 and l_2 appear in the theory.

The appropriate solutions to equations (9.2.22) for the problem under study are given by

$$\Phi = \frac{T}{4}r^2(1-\cos 2\theta) + A_1 \log r + \left(\frac{A_2}{r^2} + A_3\right)\cos 2\theta$$
$$\Psi = \left(\frac{A_4}{r^2} + A_5 K_2\left(\frac{r}{l_1}\right)\right)\sin 2\theta \tag{9.2.24}$$

where K_n is the *modified Bessel function of the second kind or order n*, and A_i are constants to be determined with $A_4 = 8(1-\nu)l_1^2 A_3$. Using this stress function solution, the components of the stress and couple-stress then follow from (9.2.21) to be

$$\begin{aligned}
T_{rr} &= \frac{T}{2}(1+\cos 2\theta) + \frac{A_1}{r^2} - \left(\frac{6A_2}{r^4} + \frac{4A_3}{r^2} - \frac{6A_4}{r^4}\right)\cos 2\theta \\
&\quad + \frac{2A_5}{l_1 r}\left[\frac{3l_1}{r}K_o(r/l_1) + \left(1+\frac{6l_1^2}{r^2}\right)K_1(r/l_1)\right]\cos 2\theta \\
T_{\theta\theta} &= \frac{T}{2}(1-\cos 2\theta) - \frac{A_1}{r^2} + \left(\frac{6A_2}{r^4} - \frac{6A_4}{r^4}\right)\cos 2\theta \\
&\quad - \frac{2A_5}{l_1 r}\left[\frac{3l_1}{r}K_o(r/l_1) + \left(1+\frac{6l_1^2}{r^2}\right)K_1(r/l_1)\right]\cos 2\theta \\
T_{r\theta} &= -\left(\frac{T}{2} + \frac{6A_2}{r^4} + \frac{2A_3}{r^2} - \frac{6A_4}{r^4}\right)\sin 2\theta \\
&\quad + \frac{A_5}{l_1 r}\left[\frac{6l_1}{r}K_o(r/l_1) + \left(1+\frac{12l_1^2}{r^2}\right)K_1(r/l_1)\right]\sin 2\theta \\
T_{\theta r} &= -\left(\frac{T}{2} + \frac{6A_2}{r^4} + \frac{2A_3}{r^2} - \frac{6A_4}{r^4}\right)\sin 2\theta \\
&\quad + \frac{A_5}{l_1^2}\left[\left(1+\frac{6l_1^2}{r^2}\right)K_o(r/l_1) + \left(\frac{3l_1}{r} + \frac{12l_1^3}{r^3}\right)K_1(r/l_1)\right]\sin 2\theta \\
m_{rz} &= -\left\{\frac{2A_4}{r^3} + \frac{A_5}{l_1}\left[\frac{2l_1}{r}K_o(r/l_1) + \left(1+\frac{4l_1^2}{r^2}\right)K_1(r/l_1)\right]\right\}\sin 2\theta \\
m_{\theta z} &= \left\{\frac{2A_4}{r^3} + \frac{2A_5}{r}\left[K_o(r/l_1) + \frac{2l_1}{r}K_1(r/l_1)\right]\right\}\cos 2\theta
\end{aligned} \tag{9.2.25}$$

For boundary conditions, we use the usual forms for the nonpolar variables, while the couple stress m_{rz} is taken to vanish on the hole boundary and at infinity

$$\begin{gathered} T_{rr}(a,\theta)=T_{r\theta}(a,\theta)=m_{rz}(a,\theta)=0 \\ T_{rr}(\infty,\theta)=\frac{T}{2}(1+\cos 2\theta) \\ T_{r\theta}(\infty,\theta)=-\frac{T}{2}\sin 2\theta \\ m_{rz}(\infty,\theta)=0 \end{gathered} \tag{9.2.26}$$

Using these conditions, sufficient relations can be developed to determine the arbitrary constants A_i giving the results

$$\begin{gathered} A_1=-\frac{T}{2}a^2, \quad A_2=-\frac{Ta^4(1-F)}{4(1+F)} \\ A_3=\frac{Ta^2}{2(1+F)}, \quad A_4=\frac{4T(1-\nu)a^2l_2^2}{1+F} \\ A_5=-\frac{Tal_1F}{(1+F)K_1(a/l_1)} \end{gathered} \tag{9.2.27}$$

where

$$F=8(1-\nu)\frac{l_2^2}{l_1^2}\left[4+\frac{a^2}{l_1^2}+\frac{2a}{l_1}\frac{K_o(a/l_1)}{K_1(a/l_1)}\right]^{-1} \tag{9.2.28}$$

and the problem is now solved.

Let us now investigate the maximum stress and discuss the nature of the concentration behavior in the vicinity of the hole and compare with classical elasticity predictions. As in the previous nonpolar case, the circumferential stress $T_{\theta\theta}$ on the hole boundary will be the maximum stress. From the (9.2.25),

$$T_{\theta\theta}(a,\theta)=T\left(1-\frac{2\cos 2\theta}{1+F}\right) \tag{9.2.29}$$

As expected, the maximum value of this quantity occurs at $\theta=\pm\pi/2$, and thus the stress concentration factor for the micropolar stress problem is given by

$$K=\frac{(T_{\theta\theta})_{\max}}{T}=\frac{3+F}{1+F} \tag{9.2.30}$$

Notice that for micropolar theory, the stress concentration depends on the material parameters and on the *size of the hole*. This problem has also been solved by Mindlin (1963) for couple-stress theory, and this result may be found from the current solution by letting $l_1=l_2=l$. Fig. 9.5 illustrates the behavior of the stress concentration factor as a function of a/l_1 for several cases of length ratio l_2/l_1 with $\nu = 0$. It is observed that the micropolar/couple-stress

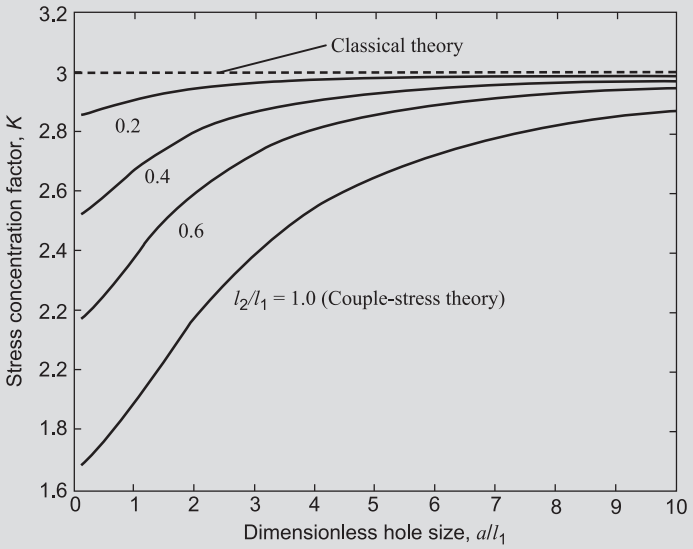

FIGURE 9.5

Stress concentration behavior for micropolar theory ($\nu = 0$).

concentration factors are *less than* that predicted by classical theory ($K = 3$), and differences between the theories depend on the ratio of the hole size to the microstructural length parameter l_j (or l). If the length parameter is small in comparison to the hole size, very little differences in the stress concentration predictions will occur. For the case $l_1 = l_2 = l = 0$, it can be shown that $F \to 0$, thus giving $K = 3$ which matches with the classical result. Mindlin (1963) also investigated other far-field loading conditions for this problem. He showed that for the case of equal biaxial loading, the couple-stress effects disappear completely, while for pure shear loading couple-stress effects produce a significant reduction in the stress concentration when compared to classical theory.

Originally, it was hoped that this solution could be used to explain the observed reduction in stress concentration factors for small holes in regions of high stress gradients. Unfortunately, it has been pointed out by several authors (Schijve, 1966; Ellis and Smith, 1967; Kaloni and Ariman, 1967) that for typical metals the reduction in the stress concentration for small holes cannot be accurately accounted for using couple-stress or micropolar theory. Additional similar solutions for stress concentrations around circular inclusions have been developed by Weitsman (1965) and Hartranft and Sih (1965).

More recent studies have had success in applying micropolar/couple-stress theory to fiber-reinforced composites (Sun and Yang, 1975) and granular materials (Chang and Ma, 1991). With respect to computational methods, micropolar finite-element techniques have been developed by Kennedy and Kim (1987) and Kennedy (1999). Many other published research papers have appeared dealing with various applications and developments of this microelasticity theory.

9.3 ELASTICITY THEORY WITH VOIDS

Another interesting micromechanics model has been proposed for porous and granular materials with distributed voids. Originally developed by Goodman and Cowin (1972) for more general materials, we focus here only on the linear elastic theory which was given by Cowin and Nunziato (1983). A series of application papers followed including Cowin and Puri (1983), Cowin (1984a,b), and Cowin (1985a). The theory is intended for elastic materials containing a uniform distribution of small voids as shown in Fig. 9.6. When the void volume vanishes, the material behavior reduces to classical elasticity theory. The primary feature of the new theory is the introduction of a volume fraction (related to void volume), which is taken as an *independent kinematic variable*. The other variables of displacement and strain are retained in their usual form for small deformations. The inclusion of the new variable requires additional microforces to provide proper equilibrium of the micropore volume.

The theory begins by expressing the material mass density as the following product:

$$\rho = \gamma \nu \tag{9.3.1}$$

where ρ is the bulk (overall) mass density, γ is the mass density of the matrix material, and ν is the *matrix volume fraction* or *volume distribution function*. This function describes the way the medium is distributed in space and is taken to be an independent variable, thus introducing an additional kinematic degree of freedom in the theory. The linear theory with voids deals with small changes from a *stress- and strain-free reference configuration.* In this configuration, relation (9.3.1) can be written as $\rho_R = \gamma_R \nu_R$. The independent kinematical variables of this theory are the usual displacements u_i, and the *change in volume fraction* from the reference configuration expressed by

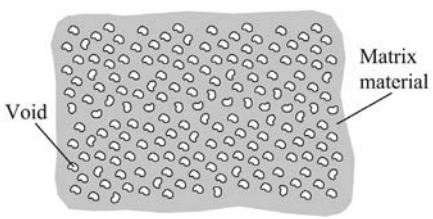

FIGURE 9.6

Solid continuum with distributed voids.

$$\phi = v - v_R \tag{9.3.2}$$

The strain displacement relations are those of classical small deformation elasticity

$$\varepsilon_{ij} = \frac{1}{2}(u_{i,j} + u_{j,i}) \tag{9.3.3}$$

and likewise for the equilibrium equations (with no body forces) reads

$$T_{ij,j} = 0 \tag{9.3.4}$$

The general development of this theory included external body forces and dynamic inertial terms, but these will not be retained in our brief presentation.

In order to develop the microequilibrium of the void volume, new micromechanics theory involving the balance of *equilibrated force* is introduced. Details of this development are beyond the scope of our presentation and we will only give the final results for the quasi-static case:

$$h_{i,i} + g = 0 \tag{9.3.5}$$

where h_i is the *equilibrated stress vector* and g is the *intrinsic equilibrated body force*. Simple physical meanings of these variables have proved difficult to provide. Cowin and Nunziato (1983) have indicated that these variables can be related to particular self-equilibrated singular force systems. In particular, h_i and g can be associated with double force systems, and the expression $h_{i,i}$ can be related to centers of dilatation (see Sadd, 2014, Chapter 15). This balance of equilibrated force has been re-examined by Fang et al. (2006) and Chen and Lan (2008), and these studies have provided some additional corrections and clarity.

The constitutive equations for linear isotropic elastic materials with voids provide relations for the stress tensor, equilibrated stress vector, and intrinsic body force of the form

$$\begin{aligned} T_{ij} &= \lambda \varepsilon_{kk}\delta_{ij} + 2\mu\varepsilon_{ij} + \beta\phi\delta_{ij} \\ h_i &= \alpha\phi_{,i} \\ g &= -\omega\dot{\phi} - \xi\phi - \beta\varepsilon_{kk} \end{aligned} \tag{9.3.6}$$

where the material constants $\lambda, \mu, \alpha, \beta, \xi, \omega$ all depend on the reference fraction v_R and satisfy the inequalities

$$\mu \geq 0, \quad \alpha \geq 0, \quad \xi \geq 0, \quad \omega \geq 0, \quad 3\lambda + 2\mu \geq 0, \quad M = \frac{3\lambda + 2\mu}{\beta^2}\xi \geq 3 \tag{9.3.7}$$

Note that even though we have dropped dynamic inertial terms, constitutive relation $(9.3.6)_3$ includes a *time-dependent response* in the volume fraction. This fact indicates that the theory will predict a *viscoelastic* type of behavior (Cowin, 1985a) even for problems with time independent boundary conditions and homogeneous deformations.

For this theory, the boundary conditions on stress and displacement are the same as those of classical elasticity. The boundary conditions on the self-equilibrated stress vector are taken to have a *vanishing normal component*, that is, $h_i n_i = 0$ where n_i is the surface unit normal vector. Using this with the constitutive statement $(9.3.6)_2$ develops the boundary specification on the volume fraction

$$\phi_{,i} n_i = 0 \tag{9.3.8}$$

This completes our brief general presentation of the theory. We will now discuss the solution to the classical two-dimensional stress concentration problem around a circular hole discussed previously.

EXAMPLE 9.3.1 ELASTICITY WITH VOIDS STRESS CONCENTRATION AROUND A CIRCULAR HOLE UNDER UNIFORM UNIAXIAL LOADING

Consider again the stress concentration problem of a stress-free circular hole of radius a in an infinite plane under uniform tension as shown in Fig. 6.12. We have previously discussed this problem for the classical elastic case in Example 6.2.4 and for the micropolar/couple-stress case in Example 9.2.1. We will now outline the solution given by Cowin (1984b) and compare the results with the micropolar/couple-stress and classical solutions.

Solution: The problem is formulated under plane stress conditions:

$$T_{xx} = T_{xx}(x,y), \quad T_{yy} = T_{yy}(x,y), \quad T_{xy} = T_{xy}(x,y), \quad T_{zz} = T_{xz} = T_{yz} = 0$$

For this two-dimensional case, the constitutive relations reduce to

$$\begin{aligned} T_{ij} &= \frac{2\mu}{\lambda + 2\mu}(\lambda \varepsilon_{kk} + \beta\phi)\delta_{ij} + 2\mu\varepsilon_{ij} \\ g &= -\omega\dot{\phi} - \left(\xi - \frac{\beta^2}{\lambda + 2\mu}\right)\phi - \frac{2\mu\beta}{\lambda + 2\mu}\varepsilon_{kk} \end{aligned} \tag{9.3.9}$$

where all indices are taken over the limited range 1, 2. Using a stress formulation, the single nonzero compatibility relation becomes

$$T_{kk,mm} - \frac{\mu\beta}{\lambda + \mu}\phi_{,mm} = 0 \tag{9.3.10}$$

Introducing the usual Airy stress function (6.2.47) denoted here by ψ allows this relation to be written as

$$\nabla^4 \psi - \frac{\mu\beta}{\lambda + \mu}\nabla^2 \phi = 0 \tag{9.3.11}$$

For this case, relation (9.3.5) for balance of equilibrated forces reduces to

$$\alpha\nabla^2\phi - \frac{\alpha}{h^2}\phi - \omega\dot{\phi} = \frac{\beta}{3\lambda + 2\mu}\left(\nabla^2\psi - \frac{\mu\beta}{\lambda + \mu}\phi\right) \tag{9.3.12}$$

The parameter h is defined by

$$\frac{\alpha}{h^2} = \xi - \frac{\beta^2}{\lambda + \mu} \tag{9.3.13}$$

and has units of length and thus can be taken as a *microstructural length measure* for this particular theory.

Relations (9.3.11) and (9.3.12) now form the governing equations for the plane stress problem. The presence of the time-dependent derivative term in (9.3.12) requires some additional analysis. Using Laplace transform theory, Cowin (1984b) has shown that under steady boundary conditions, solutions for ϕ and ψ can be determined from the limiting case where $t \to \infty$ which is related to taking $\omega = 0$. Thus, by taking the Laplace transform of (9.3.11) and (9.3.12) gives

$$\begin{aligned} \nabla^4 \bar{\psi} - \frac{\mu\beta}{\lambda+\mu}\nabla^2 \bar{\phi} &= 0 \\ \alpha \nabla^2 \bar{\phi} - \frac{\alpha}{\bar{h}^2}\bar{\phi} &= \frac{\beta}{3\lambda + 2\mu}\left(\nabla^2 \bar{\psi} - \frac{\mu\beta}{\lambda+\mu}\bar{\phi}\right) \end{aligned} \tag{9.3.14}$$

where $\bar{\phi} = \bar{\phi}(s), \bar{\psi} = \bar{\psi}(s)$ are the standard Laplace transforms of ϕ, ψ, and s is the Laplace transform variable (see Section 6.5), and the parameter $\bar{h}$ is defined by $\frac{\alpha}{\bar{h}^2} = \frac{\alpha}{h^2} + \omega s$.

Boundary conditions on the problem follow from our previous discussions to be

$$T_{rr} = T_{r\theta} = \frac{\partial \bar{\phi}}{\partial r} = 0 \text{ on } r = a$$

For the circular hole problem, the solution to system (9.3.14) is developed in polar coordinates. Guided by the results from classical elasticity, we look for solutions of the form $f_1(r) + f_2(r)\cos 2\theta$, where f_1 and f_2 are arbitrary functions of the radial coordinate. Employing this scheme, the properly bounded solution satisfying the boundary condition $\frac{\partial \bar{\phi}}{\partial r} = 0$ at $r = a$ is found to be

$$\begin{aligned} \bar{\phi} &= \frac{-\xi \bar{p}}{M\beta\omega s + \beta\xi(M-3)} + \frac{A_3(\lambda+\mu)}{\mu \bar{h}^2 \beta}[\bar{F}(r) - 1]\cos 2\theta \\ \bar{\psi} &= \frac{\mu\beta}{\lambda+\mu}\bar{h}^2\bar{\phi} + \left[\frac{\bar{p}r^2}{4} + A_1 \log r + \left(\frac{A_2}{r^2} + A_3 - \frac{\bar{p}r^2}{4}\right)\cos 2\theta\right] \end{aligned} \tag{9.3.15}$$

where $\bar{F}$ is given by

$$\bar{F}(r) = 1 + \frac{4\mu\xi\bar{h}^2}{(\lambda+\mu)M\omega s + 4\mu\xi N}\left[\frac{1}{r^2} + \frac{2\bar{h}K_2(r/\bar{h})}{a^3 K_2'(a/\bar{h})}\right] \tag{9.316}$$

and $\overline{p}$ is the Laplace transform of the uniaxial stress at infinity, K_2 is the modified Bessel function of the second kind of order 2, $N = \dfrac{\lambda+\mu}{4\mu}(M-3) \geq 0$, and the constants A_1, A_2, A_3 are determined from the stress-free boundary conditions as

$$A_1 = -\frac{1}{2}\overline{p}a^2, \quad A_2 = -\frac{1}{4}\overline{p}a^4, \quad A_3 = \frac{\overline{p}a^2}{2\overline{F}(a)}$$

Note in relation (9.3.16), the bar on F indicates the dependency on the Laplace transform parameter s, and the bar is to be removed for the case where $s \to 0$ and $\overline{h}(s)$ is replaced by h.

This completes the solution for the Laplace-transformed volume fraction and Airy stress function. The transformed stress components can now be obtained from the Airy function using the usual relations

$$\overline{T}_{rr} = \frac{1}{r}\frac{\partial\overline{\psi}}{\partial r} + \frac{1}{r^2}\frac{\partial^2\overline{\psi}}{\partial\theta^2}, \quad \overline{T}_{\theta\theta} = \frac{\partial^2\overline{\psi}}{\partial r^2}, \quad \overline{T}_{r\theta} = \frac{1}{r^2}\frac{\partial\overline{\psi}}{\partial\theta} - \frac{1}{r}\frac{\partial^2\overline{\psi}}{\partial r\partial\theta} \tag{9.3.17}$$

We will now consider the case where the far-field tension T is a constant in time, and thus $\overline{p} = T/s$. Rather than formally inverting (inverse Laplace transformation) the resulting stress components generated from relations (9.3.17), Cowin develops the results for the cases of $t = 0$ and $t \to \infty$. It turns out that for the initial condition at $t = 0$, the stresses match those found from classical elasticity (see Example 6.2.4). However, for the final-value case ($t \to \infty$), which implies ($s \to 0$), the stresses are different than predictions from classical theory.

Focusing our attention only to the hoop stress, the elasticity with voids solution for the final-value case is determined as

$$T_{\theta\theta} = \frac{T}{2}\left\{\left(1+\frac{a^2}{r^2}\right) + \cos 2\theta\left[a^2\frac{F''(r)}{F(a)} - \left(1+3\frac{a^4}{r^4}\right)\right]\right\} \tag{9.3.18}$$

The maximum value of this stress is again found at $r = a$ and $\theta = \pm\pi/2$ and is given by

$$\begin{aligned}(T_{\theta\theta})_{\max} &= T_{\theta\theta}(a, \pm\pi/2) = T\left(3 - \frac{a^2}{2}\frac{F''(a)}{F(a)}\right) \\ &= T\left[3 + \left(2N + [1+(4+L^2)N]\frac{K_1(L)}{LK_o(L)}\right)^{-1}\right]\end{aligned} \tag{9.3.19}$$

where $L = a/h$. It is observed from this relation that the stress concentration factor $K = (T_{\theta\theta})_{\max}/T$ will always be greater than or equal to 3. Thus, the elasticity theory with voids predicts an *elevation* of the stress concentration when

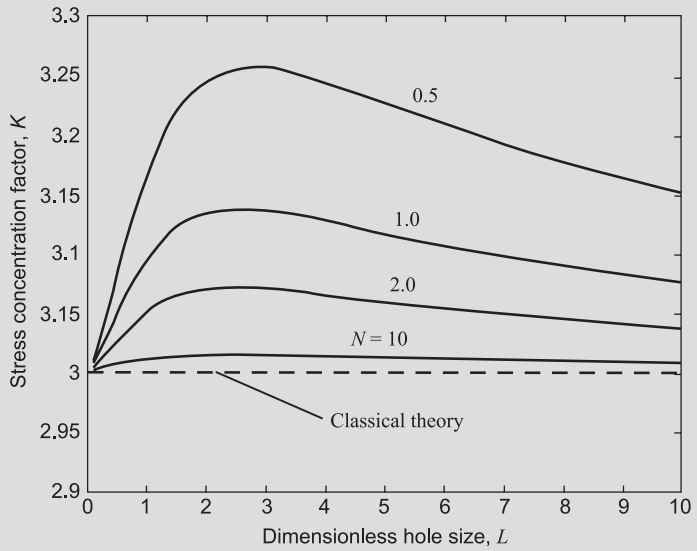

FIGURE 9.7

Stress concentration behavior for elastic material with voids.

compared to the classical result. The behavior of the stress concentration factor as a function of the dimensionless hole size L is shown in Fig. 9.7. It can be seen that the stress concentration factor reduces to the classical result as L approaches zero or infinity. For a particular value of the material parameter N, the stress concentration takes on a maximum value at a finite intermediate value of L.

It is interesting to compare these results with our previous study of the same stress concentration problem using the micropolar theory previously discussed. Recall in Example 9.2.1 we solved the identical problem for micropolar/couple-stress theories, and the results were shown in Fig. 9.5. Thus, Figs. 9.5 and 9.7 illustrate the stress concentration behavior as a function of a nondimensional ratio of hole radius divided by a microstructural length parameter. While the current model with voids indicates an elevation of stress concentration, the micropolar/couple-stress results show a decrease in this factor. Micropolar/couple-stress theory also predicts that the largest difference from the classical result occurs at a dimensionless hole size ratio of zero. However, for elasticity with voids, this difference occurs at a finite hole size ratio approximately between 2 and 3. It is apparent that micropolar theory (allowing independent microrotational deformation) will give fundamentally different results than the current void theory which allows for an independent microvolumetric deformation.

9.4 DOUBLET MECHANICS

We now wish to explore a micromechanical theory that has demonstrated applications for particulate materials in predicting observed behaviors that cannot be shown using classical continuum mechanics. The theory known as *doublet mechanics* (DM) was originally developed by Granik (1978). It has been applied to granular materials by Granik and Ferrari (1993) and Ferrari et al. (1997) and to asphalt concrete materials by Sadd and Dai (2004). DM is a micromechanical theory based on a discrete material model whereby solids are represented as arrays of points or nodes at finite distances. A pair of such nodes is referred to as a *doublet*, and the nodal spacing distances introduce *length scales* into the theory. Current applications of this scheme have normally used regular arrays of nodal spacing, thus generating a regular lattice microstructure with similarities to the micropolar model shown in Fig. 9.3. Each node in the array is allowed to have a translation and rotation, and increments of these variables are expanded in a Taylor series about the nodal point. The order at which the series is truncated defines the degree of approximation employed. The lowest order case using only a single term in the series will not contain any length scales, while using additional terms results in a multilength scale theory. The allowable kinematics develops microstrains of elongation, shear, and torsion (about the doublet axis). Through appropriate constitutive assumptions, these microstrains can be related to corresponding elongational, shear, and torsional microstresses.

Although not necessary, a *granular interpretation* of DM is commonly employed, in which the material is viewed as an assembly of circular or spherical particles. A pair of such particles represents a doublet as shown in Fig. 9.8. Corresponding to the doublet (A, B), there exists a *doublet* or *branch vector* ζ_α connecting the adjacent particle centers and defining the doublet axis α. The magnitude of this vector $\eta_\alpha = |\zeta_\alpha|$ is simply the sum of the two radii for particles in contact. However, in general, the particles need not be in contact, and the length scale η_α could be used to represent a more general microstructural feature. As mentioned, the kinematics allow relative elongational, shearing, and torsional motions between the particles, and this is used

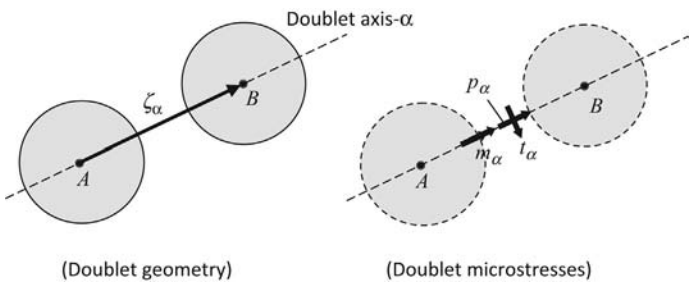

FIGURE 9.8

Doublet Mechanics geometry.

to develop *elongational microstress* $\boldsymbol{p}_\alpha$, *shear microstress* $\boldsymbol{t}_\alpha$, and *torsional microstress* $\boldsymbol{m}_\alpha$ as shown in Fig. 9.8. It should be pointed out that these microstresses are not second-order tensors in the usual continuum mechanics sense. Rather, they are vector quantities that represent the elastic microforces and microcouples of interaction between doublet particles. Their directions are dependent on the doublet axes that are determined by the material microstructure. Also, these microstresses are not continuously distributed but rather exist only at particular points in the medium being simulated by DM theory.

If $\boldsymbol{u}(\boldsymbol{x},t)$ is the displacement field coinciding with a particle displacement, then the increment function can be written as

$$\Delta \boldsymbol{u}_\alpha = \boldsymbol{u}(\boldsymbol{x}+\zeta_\alpha,t) - \boldsymbol{u}(\boldsymbol{x},t) \tag{9.4.1}$$

where $\alpha = 1,\ldots,n,$ and n is referred to as the *valence* of the lattice. Considering only the case where the doublet interactions are symmetric, it can be shown that the shear and torsional microdeformations and stresses vanish, and thus only extensional strains and stresses will exist. For this case, the extensional microstrain ε_α (representing the elongational deformation of the doublet vector) is defined by

$$\varepsilon_\alpha = \frac{\boldsymbol{q}_\alpha \cdot \Delta \boldsymbol{u}_\alpha}{\eta_\alpha} \tag{9.4.2}$$

where $\boldsymbol{q}_\alpha = \zeta_\alpha/\eta_\alpha$ is the unit vector in the α-direction. The increment function (9.4.1) can be expanded in a Taylor series as

$$\Delta \boldsymbol{u}_\alpha = \sum_{m=1}^{M} \frac{(\eta_\alpha)^m}{m!} (\boldsymbol{q}_\alpha \cdot \nabla)^m \boldsymbol{u}(\boldsymbol{x},t) \tag{9.4.3}$$

Using this result in relation (9.4.2) develops the series expansion for the extensional microstrain

$$\varepsilon_\alpha = q_{\alpha i} \sum_{m=1}^{M} \frac{(\eta_\alpha)^{m-1}}{m!} q_{\alpha k_1} \cdots q_{\alpha k_m} \frac{\partial^m u_i}{\partial x_{k_1} \ldots \partial x_{k_m}} \tag{9.4.4}$$

where $q_{\alpha k}$ are the direction cosines of the doublet directions with respect to the coordinate system. As mentioned, the number of terms used in the series expansion of the local deformation field determines the order of approximation in DM theory. For the first-order case ($m = 1$), the scaling parameter η_α will drop from the formulation, and the elongational microstrain is reduced to

$$\varepsilon_\alpha = q_{\alpha i} q_{\alpha j} \varepsilon_{ij} \tag{9.4.5}$$

where ε_{ij} is the usual small strain tensor. For this case, it has been shown that the DM solution can be calculated directly from the corresponding continuum elasticity solution through the relation

$$T_{ij} = \sum_{\alpha=1}^{n} q_{\alpha i} q_{\alpha j} p_\alpha \tag{9.4.6}$$

For the two-dimensional case, this result can be expressed in matrix form

$$\boldsymbol{T} = \boldsymbol{Q}\boldsymbol{p} \Rightarrow \boldsymbol{p} = \boldsymbol{Q}^{-1}\boldsymbol{T} \tag{9.4.7}$$

where $\boldsymbol{T} = \{T_{xx}, T_{yy}, T_{xy}\}^T$ is the continuum elastic stress vector in Cartesian coordinates, $\boldsymbol{p}$ is the microstress vector, and $\boldsymbol{Q}$ is a transformation matrix. For plane problems, this transformation matrix can be written as

$$\boldsymbol{Q} = \begin{bmatrix} (q_{11})^2 & (q_{21})^2 & (q_{31})^2 \\ (q_{12})^2 & (q_{22})^2 & (q_{32})^2 \\ q_{11}q_{12} & q_{21}q_{22} & q_{31}q_{32} \end{bmatrix} \tag{9.4.8}$$

This result allows a straightforward development of first-order DM solutions for many problems of engineering interest.

EXAMPLE 9.4.1 DM SOLUTION OF THE ELASTICITY FLAMANT PROBLEM

We now wish to investigate a specific application of the DM model for a two-dimensional problem with regular particle packing microstructure. The case of interest is the Flamant problem of a concentrated force acting on the free surface of a semi-infinite solid as shown in Fig. 9.9. The classical elasticity solution to this problem was originally developed in Example 6.2.5, and the Cartesian stress distribution was given by relations (6.2.67):

$$\begin{aligned} T_{xx} &= -\frac{2Px^2y}{\pi(x^2+y^2)^2} \\ T_{yy} &= -\frac{2Py^3}{\pi(x^2+y^2)^2} \\ T_{xy} &= -\frac{2Pxy^2}{\pi(x^2+y^2)^2} \end{aligned} \tag{9.4.9}$$

This continuum mechanics solution specifies that the normal stresses are *everywhere compressive* in the half space ($y > 0$), and a plot of the distribution of normal and shear stresses on a surface y = constant was shown in Fig. 6.15.

The DM model of this problem is established by choosing a regular two-dimensional hexagonal packing as shown in Fig. 9.9. This geometrical microstructure establishes three doublet axes at angles $\gamma = 60°$ as shown. Using only first-order approximation, DM shear and torsional microstresses vanish, leaving only elongational microstress components (p_1, p_2, p_3) as shown. Positive elongational components correspond to tensile forces between particles.

For this fabric geometry, the transformation matrix (9.4.8) becomes

$$\boldsymbol{Q} = \begin{bmatrix} \cos^2\gamma & \cos^2\gamma & 1 \\ \sin^2\gamma & \sin^2\gamma & 0 \\ -\cos\gamma\sin\gamma & \cos\gamma\sin\gamma & 0 \end{bmatrix} \tag{9.4.10}$$

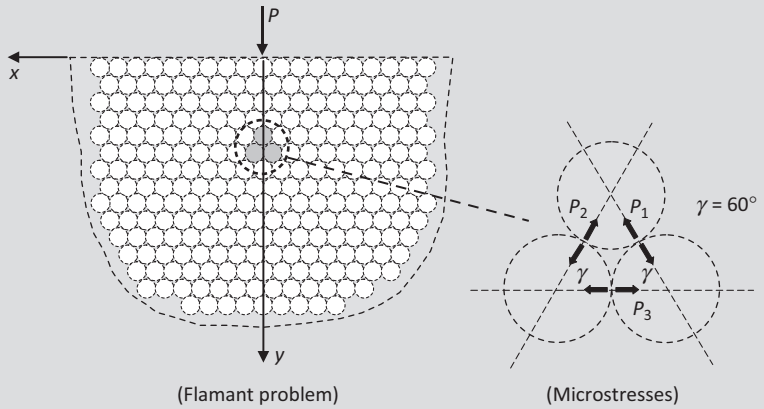

FIGURE 9.9

Flamant problem for the Doublet Mechanics model.

Using this transformation in relation (9.4.7) produces the following microstresses:

$$p_1 = -\frac{4Py^2(\sqrt{3}x+y)}{3\pi(x^2+y^2)^2}$$
$$p_2 = -\frac{4Py^2(\sqrt{3}x-y)}{3\pi(x^2+y^2)^2} \qquad (9.4.11)$$
$$p_3 = -\frac{2Py(3x^2-y^2)}{3\pi(x^2+y^2)^2}$$

Although these DM microstresses actually exist only at discrete points and in specific directions as shown in Fig. 9.9, we will use these results to make continuous contour plots over the half-space domain under study. In this fashion, we can compare DM predictions with the corresponding classical elasticity results. Reviewing the stress fields given by (9.4.9) and (9.4.11), we can only directly compare the horizontal elasticity component with the DM microstress p_3. The other stress components act in different directions, and thus do not allow a simple direct comparison.

Fig. 9.10 illustrates contour plots of the elasticity T_{xx} and DM p_3 stress components. As mentioned previously, the classical elasticity results predict a totally compressive stress field as shown. Note, however, the difference in predictions from DM theory. There exists a symmetric region of tensile microstress below the loading point in region $y \geq \sqrt{3}\,|x|$. It has been pointed out in the literature that there exists experimental evidence of such tensile behavior in granular and particulate composite materials under similar surface loading, and Ferrari et al. (1997) refer to this issue as *Flamant's paradox*. It would appear that micromechanical effects are the mechanisms for the observed tensile behaviors, and DM theory offers a possible approach to predict this phenomenon. Note that our comparisons are of qualitative nature. Additional anomalous elastic behaviors have been reported for other plane elasticity problems (Ferrari et al., 1997; Sadd and Dai, 2004).

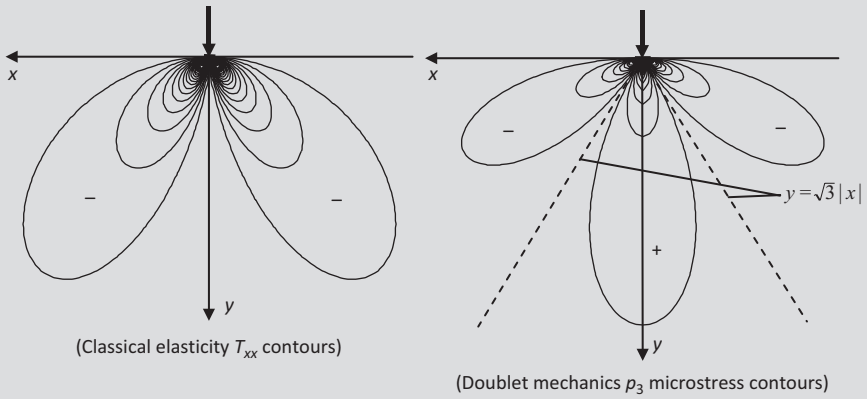

FIGURE 9.10

Comparison of horizontal stress fields from classical elasticity and Doublet Mechanics.

9.5 HIGHER GRADIENT ELASTICITY THEORIES

In classical elasticity, the strain energy can be expressed as a quadratic function of the infinitesimal strain tensor $U = U(\varepsilon_{ij})$, and thus the stress $T_{ij} = \partial U / \partial \varepsilon_{ij}$ will be a linear function of the strain. With interest in microstructural behavior and especially focusing on finding better ways to model singularities, localization, and size effects, researchers began to explore new expanded elasticity theories that would also include higher gradients of strain in the constitutive relation. These approaches have become known as *higher grade continua theories*. In addition to his work on micropolar elasticity, Mindlin (1965) was one of the originators of higher gradient theories, and he developed a linear elasticity theory that included the strain and its first and second derivatives in the constitutive relation for stress. It was anticipated that such theories would possibly remove various singularities in the solution field variables, thereby producing a more acceptable model of real materials. Starting in the 1980s, Afantis and coworkers began significant and very extensive research in this field now called *gradient elasticity theory*. Extensions to the inelastic response and other behaviors have also been included within the theory. Countless papers have been published in this field, and Aifantis (2003) and Askes and Aifantis (2011) have provided review articles on many of the more recent developments and applications of this higher-grade continua research.

For the isotropic case, Mindlin (1965) expressed the strain energy in terms of the usual strain and also included a sizeable list of first and second derivatives of the strain:

$$U = \frac{1}{2}\lambda\varepsilon_{ii}\varepsilon_{jj} + \mu\varepsilon_{ij}\varepsilon_{ij} + a_1\varepsilon_{ij,j}\varepsilon_{ik,k} + \cdots + b_1\varepsilon_{ii,jj}\varepsilon_{kk,ll} + \cdots \tag{9.5.1}$$

Using the usual hyperelastic relation, the stress can be computed for a particular case as

$$T_{ij} = \frac{\partial U}{\partial \varepsilon_{ij}} = \lambda \varepsilon_{kk}\delta_{ij} + 2\mu\varepsilon_{ij} + c_1\varepsilon_{kk,ll}\delta_{ij} + c_2\varepsilon_{ij,kk} + \frac{1}{2}c_3(\varepsilon_{kk,ij} + \varepsilon_{kk,ji}) \tag{9.5.2}$$

where λ and μ are the usual elastic constants and c_i being new material constants. Aifantis and others have generally simplified this constitutive form into

$$T_{ij} = \lambda \varepsilon_{kk}\delta_{ij} + 2\mu\varepsilon_{ij} - c[\lambda \varepsilon_{kk}\delta_{ij} + 2\mu\varepsilon_{ij}]_{,ll} \tag{9.5.3}$$

where c is the remaining single gradient material constant which has units of length squared, and hence $\sqrt{c}$ would represent a *length measure*. We thus now have a linear elastic theory that contains the usual strain terms *and second-order gradients in the strain tensor*. Over the years, other different and often more complicated constitutive forms have been developed. However, these are beyond the level and purpose of the text and thus we will limit our further study using only constitutive form (9.5.3). The remaining elasticity field equations of strain–displacement, compatibility, and equilibrium stay the same.

Following Ru and Aifantis (1993), we can establish a simple relationship between the gradient theory (9.5.3) and classical elasticity. First, noting that constitutive law (9.5.3) can be expressed in direct notational and operator form

$$\boldsymbol{T} = (1 - c\nabla^2)\boldsymbol{T}^0, \quad \boldsymbol{T}^0 = (\lambda \boldsymbol{I} tr + 2\mu)\varepsilon \tag{9.5.4}$$

where fields marked by $(\,)^0$ correspond to classical elasticity. Thus, in the absence of body forces, the equilibrium equations can be expressed by

$$\nabla \cdot \boldsymbol{T} = (1 - c\nabla^2)\nabla \cdot \boldsymbol{T}^0 = 0 \tag{9.5.5}$$

Considering the displacement form of the equilibrium equations (6.2.38), we can then write

$$(1 - c\nabla^2)\boldsymbol{L}\boldsymbol{u} = 0, \quad \boldsymbol{L} = \mu\nabla^2 + (\lambda + \mu)\nabla\nabla. \tag{9.5.6}$$

and it is noted that $\boldsymbol{L}\boldsymbol{u}^0 = 0$. Combining these results together generates the relation

$$(1 - c\nabla^2)\boldsymbol{u} = \boldsymbol{u}^0 \tag{9.5.7}$$

Thus, the gradient and classical solutions are related, and (9.5.7) provides a convenient solution scheme for gradient problems if one already knows the corresponding classical solution.

Special boundary conditions for this gradient theory are somewhat involved, and we will avoid a detailed development of this issue. Commonly an extra boundary condition for this theory is to also specify that the second normal derivative of the displacement vanishes, that is, $\partial^2 \boldsymbol{u} / \partial n^2 = 0$.

Before heading into the example problems, it should be pointed out that by incorporating higher strain gradients into constitutive relations, we inherently create a *nonsimple material* in the Noll sense. This is so because by using higher-order derivatives,

we imply a *nonlocal model*. For example, consider the one-dimensional case where the displacement difference can be expressed to first and second orders by the two relations:

$$\begin{aligned} u(x+dx)-u(x) &= \frac{du}{dx}dx = \varepsilon\, dx \\ u(x+dx)-u(x) &= \frac{du}{dx}dx + \frac{d^2u}{dx^2}(dx)^2 = \varepsilon\, dx + \frac{d\varepsilon}{dx}(dx)^2 \end{aligned} \tag{9.5.8}$$

The first-order case $(9.5.8)_1$ corresponds to usual modeling valid in a small neighborhood where $dx << 1$. However, the second case $(9.5.8)_2$ expresses the same quantity but includes the higher-order term $\frac{d\varepsilon}{dx}(dx)^2$ that incorporates a higher derivative of strain with $(dx)^2$, thereby implying the use of a larger value of dx. This fact implies that some nonlocal effects will now come into the analysis.

Nonlocal continuum elasticity theories have been developed by Eringen (1972, 1977, 1983). They postulate that the stress at location $\boldsymbol{x}$ depends not only on the strain at $\boldsymbol{x}$, but also on the strain in a neighborhood of $\boldsymbol{x}$. In this sense, the nonlocal theory incorporates *longer range actions* between material points, and such interactions have been found to exist in atomic lattices and in granular materials. For isotropic materials, the constitutive relation for the stress can thus be written as

$$T_{ij}(\boldsymbol{x}) = \int_V (\lambda(|\boldsymbol{x}'-\boldsymbol{x}|)\varepsilon_{kk}(\boldsymbol{x}')\delta_{ij} + 2\mu(|\boldsymbol{x}'-\boldsymbol{x}|)\varepsilon_{ij}(\boldsymbol{x}'))\,dV(\boldsymbol{x}') \tag{9.5.9}$$

where now the usual elastic constants λ and μ become spatial functions of the distance variable $|\boldsymbol{x}'-\boldsymbol{x}|$. The integral in relation (9.5.9) can be expanded in a series of spatial derivatives of the strain which gives constitutive forms similar to our gradient theories. Other methods have specified simplified forms for the kernel integrand functions that allow solutions to be made for particular problems.

Numerous solutions using the gradient elastic constitutive laws have been developed. We now will explore a couple of these and compare solutions with the corresponding classical elasticity case. This will allow us to examine the differences and to determine some of the effects specific of gradient theory.

EXAMPLE 9.5.1 GRADIENT ELASTICITY SOLUTION TO SCREW DISLOCATION IN THE *Z*-DIRECTION

Consider the elasticity problem of a screw dislocation in the z-direction. This is a type of internal defect in a solid that corresponds to a jump discontinuity of displacement. For a screw dislocation, the displacement field has the special form of antiplane strain where

$$u = v = 0, \quad w = w(x, y) \tag{9.5.10}$$

The problem geometry and jump in displacement are shown in Fig. 9.11.

Solution: We follow the gradient elasticity solution that has been given by Gutkin and Aifantis (1996). For the antiplane strain displacement field, the

only two nonzero strains are given by Sadd (2014):

$$\varepsilon_{xz} = \frac{1}{2}\frac{\partial w}{\partial x}, \quad \varepsilon_{yz} = \frac{1}{2}\frac{\partial w}{\partial y} \tag{9.5.11}$$

Using the gradient constitutive law (9.5.3), the only two nonzero stresses are

$$T_{xz} = \mu \frac{\partial}{\partial x}\left[w - c\left(\frac{\partial^2 w}{\partial x^2} + \frac{\partial^2 w}{\partial y^2} \right) \right], \quad T_{yz} = \mu \frac{\partial}{\partial y}\left[w - c\left(\frac{\partial^2 w}{\partial x^2} + \frac{\partial^2 w}{\partial y^2} \right) \right] \tag{9.5.12}$$

The equilibrium equations reduce to the single relation

$$\frac{\partial T_{xz}}{\partial x} + \frac{\partial T_{yz}}{\partial y} = 0 \tag{9.5.13}$$

and using (9.5.12) this gives the governing equation for the w-displacement

$$\frac{\partial^2 w}{\partial x^2} + \frac{\partial^2 w}{\partial y^2} - c\left(\frac{\partial^4 w}{\partial x^4} + 2\frac{\partial^4 w}{\partial x^2 \partial y^2} + \frac{\partial^4 w}{\partial y^4} \right) = 0 \tag{9.5.14}$$

This equation can be solved using Fourier transforms. We omit the details of such an analysis and only quote the final result

$$w = \frac{b}{2\pi}\left[\tan^{-1}\left(\frac{y}{x} \right) + \operatorname{sgn}(y) \int_0^\infty \frac{\xi \sin \xi x}{\xi^2 + 1/c} e^{-|y|\sqrt{\xi^2 + 1/c}}\, d\xi \right] \tag{9.5.15}$$

where b denotes the *Burgers vector* specifying the magnitude of the discontinuous displacement (see Fig. 9.11). This displacement gives the following strain components:

$$\begin{aligned} \varepsilon_{xz} &= \frac{b}{4\pi}\left[-\frac{y}{r^2} + \frac{y}{r\sqrt{c}} K_1\left(\frac{r}{\sqrt{c}} \right) \right] \\ \varepsilon_{yz} &= \frac{b}{4\pi}\left[\frac{x}{r^2} + \frac{x}{r\sqrt{c}} K_1\left(\frac{r}{\sqrt{c}} \right) \right] \end{aligned} \tag{9.5.16}$$

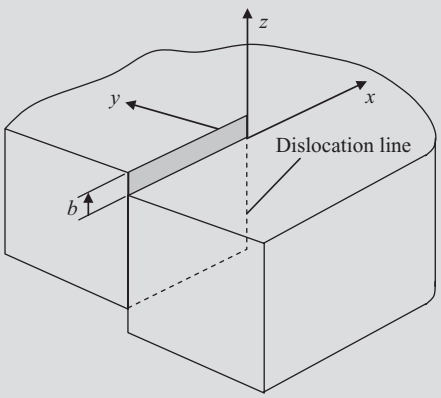

FIGURE 9.11

Screw dislocation geometry.

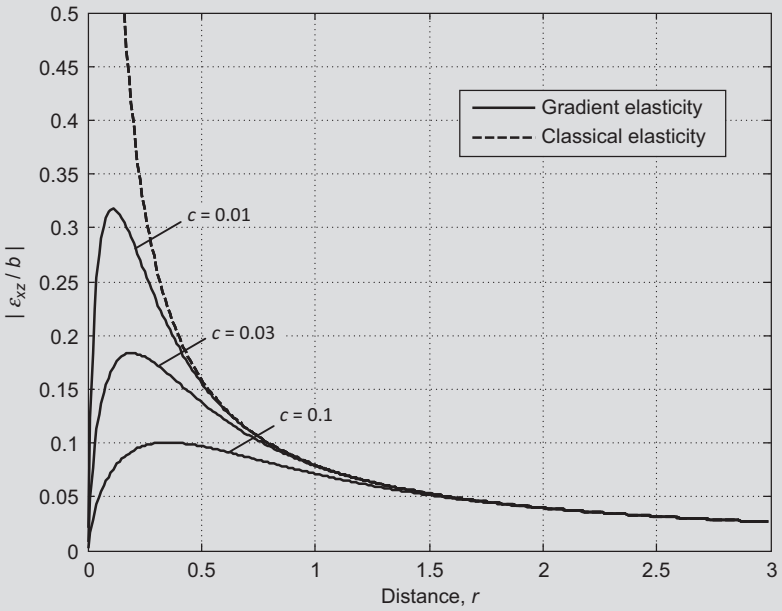

FIGURE 9.12

Local shear strain ε_{xz} behavior for a screw dislocation.

with $r = \sqrt{x^2 + y^2}$ and K_1 being the modified Bessel function of the second kind of order 1. In regard to the classical elasticity solution, the corresponding results are given by Sadd (2014):

$$w = \frac{b}{2\pi}\tan^{-1}\left(\frac{y}{x}\right), \quad \varepsilon_{xz} = -\frac{b}{4\pi}\frac{y}{r^2}, \quad \varepsilon_{yz} = \frac{b}{4\pi}\frac{x}{r^2} \tag{9.5.17}$$

From the structure of the displacement, strain, and stress solution fields, it is apparent that the gradient solution contains the classical solution plus an additive term due to the new model. This result is consistent with the findings of Ru and Aifantis (1993) for general boundary value problems of this theory. Using MATLAB Code C-23 for calculations and plotting, Fig. 9.12 illustrates the spatial behaviors of the strain component ε_{xz} for each theory. It is clearly seen that the gradient theory removes the singular behavior for the strain components (and also for the stresses). Note that the gradient strain and stress predications go to zero at the dislocation interface ($r = 0$). The removal of singular behaviors from classical elasticity is a common occurrence when using gradient theories.

EXAMPLE 9.5.2 GRADIENT ELASTICITY SOLUTION TO FLAMANT PROBLEM

Consider again the Flamant problem as shown in Fig. 6.14 which represents a point force or line load P acting normally to the free surface of an elastic half-space. Under a plane strain assumption, we wish to determine the gradient elasticity solution and compare particular features with the classical solution previously given in Example 6.2.5.

Solution: For this problem, we follow the solution developed by Li et al. (2004). They formulated the problem in two-dimensional *plane strain* with

$$u = u(x, y), \quad v = v(x, y), \quad w = 0 \tag{9.5.18}$$

which gives the following strain field:

$$\varepsilon_x = \frac{\partial u}{\partial x}, \quad \varepsilon_y = \frac{\partial v}{\partial y}, \quad \varepsilon_{xy} = \frac{1}{2}\left(\frac{\partial u}{\partial y} + \frac{\partial v}{\partial x}\right), \quad \varepsilon_z = \varepsilon_{xz} = \varepsilon_{yz} = 0 \tag{9.5.19}$$

For this deformation, the stresses follow from constitutive law (9.5.3):

$$\begin{aligned}
T_{xx} &= \lambda(\varepsilon_x + \varepsilon_y) + 2\mu\varepsilon_x - c\left[\lambda(\varepsilon_x + \varepsilon_y) + 2\mu\varepsilon_x\right]_{,mm} \\
T_{yy} &= \lambda(\varepsilon_x + \varepsilon_y) + 2\mu\varepsilon_y - c\left[\lambda(\varepsilon_x + \varepsilon_y) + 2\mu\varepsilon_y\right]_{,mm} \\
T_{zz} &= \lambda(\varepsilon_x + \varepsilon_y) - c\left[\lambda(\varepsilon_x + \varepsilon_y)\right]_{,mm} \\
T_{xy} &= 2\mu\varepsilon_{xy} - 2\mu c\left[\lambda(\varepsilon_x + \varepsilon_y)\right]_{,mm} \\
T_{yz} &= T_{xz} = 0
\end{aligned} \tag{9.5.20}$$

Combining (9.5.19) into (9.5.20), and then inserting this result into the equilibrium equations gives

$$\begin{aligned}
&\mu\nabla^2 u + (\lambda+\mu)\frac{\partial}{\partial x}\left(\frac{\partial u}{\partial x} + \frac{\partial v}{\partial y}\right) + c\nabla^2\left[\mu\nabla^2 u + (\lambda+\mu)\frac{\partial}{\partial x}\left(\frac{\partial u}{\partial x} + \frac{\partial v}{\partial y}\right)\right] = 0 \\
&\mu\nabla^2 v + (\lambda+\mu)\frac{\partial}{\partial y}\left(\frac{\partial u}{\partial x} + \frac{\partial v}{\partial y}\right) + c\nabla^2\left[\mu\nabla^2 v + (\lambda+\mu)\frac{\partial}{\partial y}\left(\frac{\partial u}{\partial x} + \frac{\partial v}{\partial y}\right)\right] = 0
\end{aligned} \tag{9.5.21}$$

This system of equations can again be solved by Fourier transforms, and details are provided in Li et al. (2004). Extracting the solution for the in-plane stresses

$$\begin{aligned}
T_{xx} &= -\frac{P}{\pi}\int_0^\infty (1-\xi y)e^{-\xi y}\cos(\xi x)\,\mathrm{d}\xi = -\frac{2Px^2 y}{\pi(x^2+y^2)^2} \\
T_{yy} &= -\frac{P}{\pi}\int_0^\infty (1+\xi y)e^{-\xi y}\cos(\xi x)\,\mathrm{d}\xi = -\frac{2Py^3}{\pi(x^2+y^2)^2} \\
T_{xy} &= -\frac{P}{\pi}\int_0^\infty \xi y\, e^{-\xi y}\sin(\xi x)\,\mathrm{d}\xi = -\frac{2Pxy^2}{\pi(x^2+y^2)^2}
\end{aligned} \tag{9.5.22}$$

which surprisingly turn out to be the same as the classical elasticity results (see Eqs. (6.2.67)). Ru and Aifantis (1993) have shown that gradient problems of this type and boundary condition have this general feature of stress field solutions matching the classical prediction.

It should be pointed out that a more recent study of this problem by Lazar and Maugin (2006) using a different set of boundary conditions claims that *both* the gradient elastic stresses and displacements are free of singularities. Since Li et al. (2004) did not provide a finalized detailed displacement solution, we will choose the equivalent results from Lazar and Maugin (2006). They give the following relation for the vertical displacement:

$$v(x,y) = \frac{P}{2\pi\mu}\left[2(1-\nu)(\log r + K_0(r/\sqrt{c}) - \frac{x^2}{r^2} + \frac{x^2-y^2}{r^2}\left(\frac{2c}{r^2} - K_2(r/\sqrt{c})\right)\right] \tag{9.5.23}$$

where again $K_{0,2}$ are the modified Bessel functions of the second kind of orders 0 and 2.

We now wish to further explore this result on free surface $y = 0$. The corresponding prediction from classical elasticity is given by

$$v(x,0) = \frac{P(1-\nu)}{\pi\mu}\log x + v_o \tag{9.5.24}$$

where v_o is an arbitrary rigid-body vertical displacement, and in fact solution (9.5.23) should also include such a term. Note the logarithmic singularity in the classical prediction.

Using MATLAB Code C-24 for calculations and plotting, these vertical surface displacement relations are shown in Fig. 9.13 for the case $\nu = 0.3$ and $c = 0.1$. The displacements are normalized with respect to the factor $\frac{P(1-\nu)}{\pi\mu}$. Unlike the stresses, displacement results indicate that the gradient solution does not match with the classical prediction. More importantly, the logarithmic singularity at the loading point in classical elasticity (Sadd, 2014) is not found, and the gradient theory predicts a finite value directly under the loading point. Again we see that gradient elasticity eliminates a singular behavior found in classical theory.

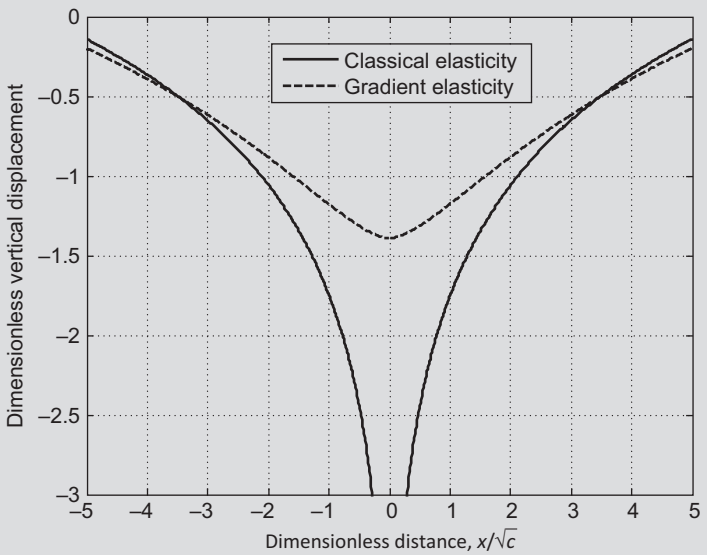

FIGURE 9.13

Dimensionless vertical surface displacement comparison for the Flamant problem with $\nu = 0.3$ and $c = 0.1$.

Examination of the published literature on gradient elasticity indicates a variety of constitutive choices which lead to different results for a given problem. In some cases, singular behaviors are removed from the classical predictions, whereas in other cases they are not. Many additional problems in gradient elasticity have appeared in the literature and no doubt new developments of this theory will continue. With respect to other continuum mechanics areas, gradient theories have also had many applications in plasticity, viscoplasticity, and localization problems.

9.6 FABRIC THEORIES FOR GRANULAR MATERIALS

Granular materials are an important class of discrete media that are composed of a large collection of independent particles or grains as shown in Fig. 9.14. Such materials include powders, sands, rocks, food grains, and other types of particulate systems. These materials will have void space that could be filled with air or a fluid. Each particle has immediate neighbors that make contact and thus affect the forces and motions (displacements and rotations) of the particle. This internal force/moment system within the granular assembly is primarily dependent on the packing geometry. Because of these and other features, many claim that granular materials are one of the most complicated media known, exhibiting localization, surface instabilities, solid–fluid transition, dilatancy, initial and induced anisotropy, microstructural response, and other complex behaviors.

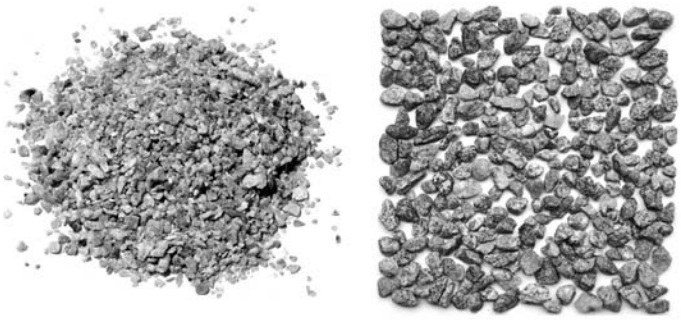

FIGURE 9.14

Examples of granular material.

The behavior of a granular material is inherently related to the internal microstructural packing geometry of the grains. The term *fabric* is often used to describe this geometry, and some typical fabric measures are shown in Fig. 9.15 that include the *particle size and shape*, *branch vectors* $\boldsymbol{l}$ that go between adjacent particle mass centers, *contact normal vectors* $\boldsymbol{n}$ that act perpendicular to surface contact points, and *void geometry* that would measure particular aspects of each void. Experimental schemes using photoelasticity on transparent model granular assemblies have shown that material fabric plays an important role in load transfer. Observations indicate that granular microstructure produces well-defined loading chains that transfer most of the forces through the material. A simple example of this effect is shown in Fig. 9.16 where two granular packing geometries are loaded by an identical central vertical load. Photoelastic data on these two assemblies would indicate that although some load transfer would be distributed in other

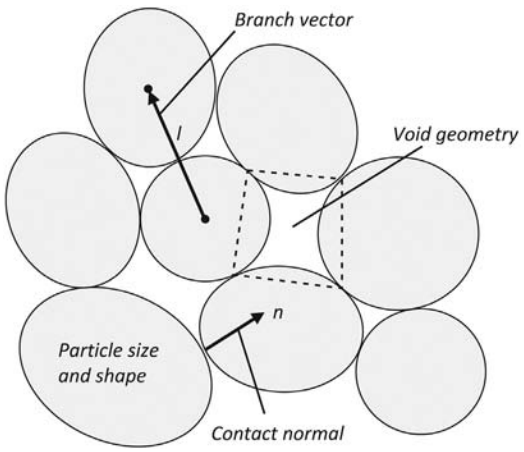

FIGURE 9.15

Typical local fabric in granular media.

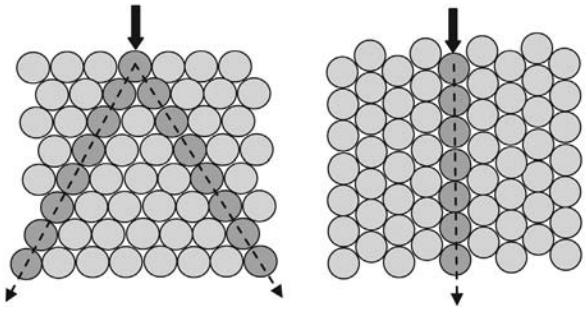

FIGURE 9.16

Fabric effects on load transfer in granular materials.

grains, the primary load transfer would occur along the shaded particles as shown. Thus, load transfer and stress distribution in granular materials is highly dependent on the material fabric. This situation is in strong contrast to the way a continuous medium would transfer such applied loading (see the linear elastic Flamant problem in Example 6.2.5).

Continuum descriptions of granular materials have employed a very large collection of schemes including various micropolar, higher gradient, and void and fabric tensor theories. Computational methods have used *discrete element modeling* with great success (Cundall and Strack, 1979). Here, we will briefly present some basic concepts of using fabric tensor theories to simulate dry granular material behavior under static equilibrium conditions.

We start with an interesting application developed by Cowin (1985b) that established a relationship between the continuum elasticity tensor and a fabric tensor. The beginning step is the assumption that there exists a *symmetric second-order fabric tensor* $\boldsymbol{M}$ that characterizes the geometric components of a multistructural and/or multiphase material. While the existence of $\boldsymbol{M}$ is assumed, the precise nature of how this fabric tensor is related to the material microstructure is not specified. We will explore this issue in some detail later in the presentation. For the elastic case, we thus choose a constitutive form

$$\boldsymbol{T} = \boldsymbol{f}(\boldsymbol{\varepsilon}, \boldsymbol{M}) \tag{9.6.1}$$

where ε is the usual small deformation strain tensor and $\boldsymbol{M}$ is the fabric tensor. Since all of these tensors are symmetric and second order, using the principle of frame indifference

$$\boldsymbol{Q}\boldsymbol{f}(\boldsymbol{\varepsilon}, \boldsymbol{M})\boldsymbol{Q}^{\mathrm{T}} = \boldsymbol{f}(\boldsymbol{Q}\boldsymbol{\varepsilon}\boldsymbol{Q}^{\mathrm{T}}, \boldsymbol{Q}\boldsymbol{M}\boldsymbol{Q}^{\mathrm{T}}) \tag{9.6.2}$$

We have seen relation (9.6.2) before in Section 8.4.3 dealing with Rivlin–Ericksen fluids of grade 2. As before, we can apply the representation theorem (2.14.5) to write

$$\begin{aligned}\boldsymbol{T} = {} & f_1\boldsymbol{I} + f_2\boldsymbol{M} + f_3\boldsymbol{M}^2 + f_4\boldsymbol{\varepsilon} + f_5\boldsymbol{\varepsilon}^2 + f_6(\boldsymbol{M}\boldsymbol{\varepsilon} + \boldsymbol{\varepsilon}\boldsymbol{M}) \\ & + f_7(\boldsymbol{M}^2\boldsymbol{\varepsilon} + \boldsymbol{\varepsilon}\boldsymbol{M}^2) + f_8(\boldsymbol{M}\boldsymbol{\varepsilon}^2 + \boldsymbol{\varepsilon}^2\boldsymbol{M}) + f_9(\boldsymbol{M}^2\boldsymbol{\varepsilon}^2 + \boldsymbol{\varepsilon}^2\boldsymbol{M}^2)\end{aligned} \tag{9.6.3}$$

where the terms f_i are functions of the invariants $tr\,\boldsymbol{M}$, $tr\,\boldsymbol{M}^2$, $tr\,\boldsymbol{M}^3$, $tr\,\varepsilon$, $tr\,\varepsilon^2$, $tr\,\varepsilon^3$, $tr(\boldsymbol{M}\varepsilon)$, $tr(\boldsymbol{M}^2\varepsilon)$, $tr(\boldsymbol{M}\varepsilon^2)$, and $tr(\boldsymbol{M}^2\varepsilon^2)$. This general form must meet the requirement that $\boldsymbol{T}$ be linear in ε and vanish when $\varepsilon = 0$, thus giving the reduction

$$\boldsymbol{T} = f_1\boldsymbol{I} + f_2\boldsymbol{M} + f_3\boldsymbol{M}^2 + f_4\boldsymbol{\varepsilon} + f_6(\boldsymbol{M}\boldsymbol{\varepsilon}+\boldsymbol{\varepsilon}\boldsymbol{M}) + f_7(\boldsymbol{M}^2\boldsymbol{\varepsilon}+\boldsymbol{\varepsilon}\boldsymbol{M}^2) \tag{9.6.4}$$

with the material functions f_i reducing to the forms

$$\begin{aligned} f_1 &= a_1\,tr\,\boldsymbol{\varepsilon} + a_2\,\mathrm{tr}\,\boldsymbol{M}\boldsymbol{\varepsilon} + a_3\,tr\,\boldsymbol{M}^2\boldsymbol{\varepsilon} \\ f_2 &= d_1\,tr\,\boldsymbol{\varepsilon} + b_1\,\mathrm{tr}\,\boldsymbol{M}\boldsymbol{\varepsilon} + b_2\,tr\,\boldsymbol{M}^2\boldsymbol{\varepsilon} \\ f_3 &= d_2\,tr\,\boldsymbol{\varepsilon} + d_3\,tr\,\boldsymbol{M}\boldsymbol{\varepsilon} + b_3\,tr\,\boldsymbol{M}^2\boldsymbol{\varepsilon} \\ f_4 &= 2c_1, \quad f_6 = 2c_2, \quad f_7 = 2c_3 \end{aligned} \tag{9.6.5}$$

where a_i, b_i, c_i, and d_i are functions of $tr\,\boldsymbol{M}$, $tr\,\boldsymbol{M}^2$, and $tr\,\boldsymbol{M}^3$. Using these results, we can now express the stress in index notation as

$$\begin{aligned} T_{ij} = {} & \delta_{ij}(a_1\varepsilon_{kk} + a_2M_{rp}\varepsilon_{pr} + a_3M_{rq}M_{qp}\varepsilon_{pr}) \\ & + M_{ij}(d_1\varepsilon_{kk} + b_1M_{rp}\varepsilon_{pr} + b_2M_{rq}M_{qp}\varepsilon_{pr}) \\ & + M_{is}M_{sj}(d_2\varepsilon_{kk} + d_3M_{rp}\varepsilon_{pr} + b_3M_{rq}M_{qp}\varepsilon_{pr}) \\ & + 2c_1\varepsilon_{ij} + 2c_2(M_{ir}\varepsilon_{rj} + \varepsilon_{ir}M_{rj}) \\ & + 2c_3(M_{ip}M_{pr}\varepsilon_{rj} + \varepsilon_{ir}M_{rp}M_{pj}) \end{aligned} \tag{9.6.6}$$

Now for linear elastic materials, the constitutive form in terms of the elasticity tensor $\boldsymbol{C}$ is given by

$$T_{ij} = C_{ijkl}\varepsilon_{kj}, \quad \text{with symmetries}\, C_{ijkl} = C_{jikl} = C_{ijlk} = C_{klij} \tag{9.6.7}$$

Comparing relations (9.6.6) with (9.6.7) and invoking the appropriate symmetries gives the following relationship between the elasticity and fabric tensors:

$$\begin{aligned} C_{ijkl} = {} & a_1\delta_{ij}\delta_{kl} + a_2(M_{ij}\delta_{kl} + \delta_{ij}M_{kl}) + a_3(\delta_{ij}M_{kq}M_{ql} + \delta_{kl}M_{iq}M_{qj}) \\ & + b_1M_{ij}M_{kl} + b_2(M_{ij}M_{kq}M_{ql} + M_{is}M_{sj}M_{kl}) + b_3M_{is}M_{sj}M_{kq}M_{ql} \\ & + c_1(\delta_{ki}\delta_{lj} + \delta_{li}\delta_{kj}) + c_2(M_{ik}\delta_{lj} + M_{kj}\delta_{li} + M_{il}\delta_{kj} + M_{lj}\delta_{ki}) \\ & + c_3(M_{ir}M_{rk}\delta_{lj} + M_{kr}M_{rj}\delta_{li} + M_{ir}M_{rl}\delta_{kj} + M_{lr}M_{rj}\delta_{ik}) \end{aligned} \tag{9.6.8}$$

and thus the final constitutive form for the stress in terms of the strain and fabric tensor is given by

$$\begin{aligned} T_{ij} = {} & a_1\delta_{ij}\varepsilon_{kk} + a_2(M_{ij}\varepsilon_{kk} + \delta_{ij}M_{kl}\varepsilon_{kl}) + a_3(\delta_{ij}M_{kq}M_{ql}\varepsilon_{kl} + M_{iq}M_{qj}\varepsilon_{kk}) \\ & + b_1M_{ij}M_{kl}\varepsilon_{kl} + b_2(M_{ij}M_{kq}M_{ql}\varepsilon_{kl} + M_{is}M_{sj}M_{kl}\varepsilon_{kl}) + b_3M_{is}M_{sj}M_{kq}M_{ql}\varepsilon_{kl} \\ & + 2c_1\varepsilon_{kk} + 2c_2(M_{ik}\varepsilon_{kj} + M_{kj}\varepsilon_{ki}) + 2c_3(M_{ir}M_{rk}\varepsilon_{kj} + M_{kr}M_{rj}\varepsilon_{ki}) \end{aligned} \tag{9.6.9}$$

As a special case, consider the situation where the fabric tensor is isotropic so that $M_{ij} = M_o\delta_{ij}$. For this case, relation (9.6.8) gives

$$\begin{aligned} C_{1111} &= C_{2222} = C_{3333} = a_1 + 2c_1 + 2(a_2 + 2c_2)M_o + (2a_3 + b_1 + 4c_3)M_o^2 + 2b_2M_o^3 + b_3M_o^4 \\ C_{1122} &= C_{1133} = C_{2233} = a_1 + 2a_2M_o + (2a_3 + b_1)M_o^2 + 2b_2M_o^3 + b_3M_o^4 \\ C_{1212} &= C_{1313} = C_{2323} = c_1 + 2c_2M_o + 2c_3M_o^2 \end{aligned} \tag{9.6.10}$$

Now the two Lamé elastic constants in classical elasticity can be expressed as

$$\begin{aligned} C_{1111} &= C_{2222} = C_{3333} = \lambda + 2\mu \\ C_{1122} &= C_{1133} = C_{2233} = \lambda \\ C_{1212} &= C_{1313} = C_{2323} = \mu \end{aligned} \tag{9.6.11}$$

and so these elastic constants can be written in terms of the fabric tensor component M_o:

$$\begin{aligned}\lambda &= a_1 + 2a_2 M_o + (2a_3 + b_1)M_o^2 + 2b_2 M_o^3 + b_3 M_o^4 \\ \mu &= c_1 + 2c_2 M_o + 2c_3 M_o^2\end{aligned} \tag{9.6.12}$$

Other material symmetries such as orthotropic and transversely isotropic have been discussed by Cowin (1985b). However, he points out that not all possible elastic material symmetries can be represented by relation (9.6.8). Of course to apply these elegant relations, the specific nature of the fabric tensor must be determined.

Next, we move on to explore the development of particular fabric tensors and definitions of stress associated with granular materials. Major work in this area has been done by many researchers including Mehrabadi et al. (1982), Nicot and Darve (2005), Li et al. (2009), and Chang and Liu (2013). Recall that for such materials the stress is transmitted in the form of force chains through the contacting particles and this fact couples the material fabric to the load transfer. Different fabric tensors and stress definitions have been proposed, incorporating different microstructural features as shown previously in Fig. 9.15, and normally this is done on a statistical basis. What can complicate things is the fact that loading can cause new contacts to appear and old contacts to disappear, thereby changing fabric during loading. For the simplified approach, here we will disregard such situations. We will also assume that all particles are convex and thus will only transmit contact forces and not moments.

Fabric is a rather general term, and thus over the years many different geometrical parameters have been proposed to create a second-order fabric tensor. Many attempts have used some type of outer or dyadic product of a particular vector field. A few such examples are shown in Fig. 9.17 and include *particle orientation vectors* $\mathbf{v}^p$, *contact normal vectors* $\boldsymbol{n}$, and *branch vectors* $\boldsymbol{l}$. All of these vectors carry the directional ambiguity of being only defined uniquely to a line of action, and thus each would carry a ± prefix sign.

The particle orientation vector would characterize the particles nonspherical or noncircular shape through a geometric calculation that would result in an oriented vector along the principle size direction. Numerical methods exist to carry out such calculations. The magnitude of this vector can be scaled to the amount of size difference between the maximum and minimum particle lengths. However, this vector is commonly normalized as are the contact normal and branch vectors. Based on these unit vectors, fabric tensors can be expressed as an average over an appropriate RVE as

$$\begin{aligned}M_{ij}^{\mathrm{p}} &= \frac{1}{N^{\mathrm{p}}}\sum_V n_i^{\mathrm{p}} n_j^{\mathrm{p}} \\ M_{ij}^{\mathrm{c}} &= \frac{1}{N^{\mathrm{c}}}\sum_V n_i^{\mathrm{c}} n_j^{\mathrm{c}} \\ M_{ij}^{l} &= \frac{1}{N^{l}}\sum_V n_i^{l} n_j^{l}\end{aligned} \tag{9.6.13}$$

where $n_i^{\mathrm{p}}, n_i^{\mathrm{c}}, n_i^{l}$ are the unit particle orientation, contact, and branch vectors, $N^{\mathrm{p}}, N^{\mathrm{c}}, N^{l}$ are the total number of particles, contacts, and branch vectors in V, respectively. Note that each of these fabric tensors is symmetric with a unit trace.

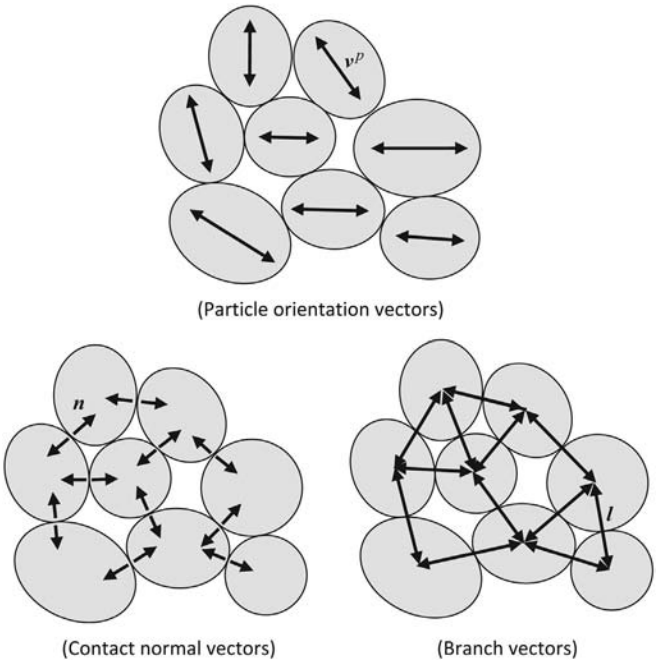

FIGURE 9.17

Example fabric vector distributions in granular media.

Now for regular granular packings like those (HCP) shown in Fig. 9.16, the fabric is completely determined if we assume no further re-arrangement with loading. Thus, the stress–strain response of such idealized cases can easily be determined based on the individual particle contact force deformation response. However, we wish to explore the more general case of a granular system with random packing of spherical particles, and this generally requires the use of a *statistical representation* of material fabric. Following the procedures outlined by Chang and Liu (2013), the *distribution of contact normals* can be expressed by a spherical harmonic Fourier expansion in the local spherical coordinate system defined in Fig. 9.18. Including just the first two terms yields

$$\xi(\phi,\theta)=\frac{1}{4\pi}\left[1+\frac{a}{4}(3\cos 2\phi+1)+3b\sin^2\phi\cos 2\theta\right] \tag{9.6.14}$$

where a and b are two constants related to the material fabric. The distribution function $\xi(\phi,\theta)$ is a probability density function that satisfies the usual condition

$$\int_0^{2\pi}\int_0^{\pi}\xi(\phi,\theta)\sin\phi\,\mathrm{d}\phi\,\mathrm{d}\theta=1 \tag{9.6.15}$$

At a typical point on the particle's surface, the three orthogonal unit vectors that coincide with the spherical basis vectors are given by

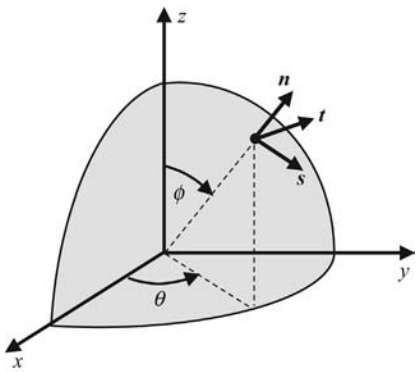

FIGURE 9.18

Local particle coordinate system.

$$\begin{aligned}\boldsymbol{n} &= \cos\phi\boldsymbol{e}_3 + \sin\phi\cos\theta\boldsymbol{e}_1 + \sin\phi\sin\theta\boldsymbol{e}_2\\ \boldsymbol{s} &= -\sin\phi\boldsymbol{e}_3 + \cos\phi\cos\theta\boldsymbol{e}_1 + \cos\phi\sin\theta\boldsymbol{e}_2\\ \boldsymbol{t} &= -\sin\theta\boldsymbol{e}_1 + \cos\theta\boldsymbol{e}_2\end{aligned} \tag{9.6.16}$$

Using relation $(9.6.16)_1$, Eq. (9.6.14) can be alternatively expressed as the Cartesian tensor expression

$$\xi(\boldsymbol{n}) = \frac{1}{4\pi} D_{ij} n_i n_j \tag{9.6.17}$$

where D_{ij} is called the *contact density tensor* and is given by

$$\boldsymbol{D} = \begin{bmatrix} 1+a & 0 & 0 \\ 0 & 1-a/2+3b & 0 \\ 0 & 0 & 1-a/2-3b \end{bmatrix} \tag{9.6.18}$$

Now we choose for our material fabric tensor to be the contact normal distribution defined by $(9.6.13)_2$, and thus $M_{ij} = \dfrac{1}{N^c}\sum_v n_i n_j$ can be expressed in terms of an integrated statistical form as

$$M_{ij} = \int_0^{2\pi}\int_0^{\pi} \xi(\phi,\theta) n_i n_j \sin\phi\, d\phi\, d\theta \tag{9.6.19}$$

Using the probability density function form from relation (9.6.14) allows (9.6.19) to be written as

$$\boldsymbol{M} = \frac{1}{15}\begin{bmatrix} 5+2a & 0 & 0 \\ 0 & 5-a+6b & 0 \\ 0 & 0 & 5-a-6b \end{bmatrix} \tag{9.6.20}$$

The force distribution in an idealized granular material is such that the *contact force or force fabric* is characterized by the orientation distribution of *interparticle contact forces*. These forces can be described by their components along the local ***n, s, t*** directions

$$\begin{aligned} f_n &= \bar{f}A_{ij} n_i n_j \\ f_s &= a_s \bar{f}A_{ij} n_i s_j \\ f_t &= a_t \bar{f}A_{ij} n_i t_j \end{aligned} \tag{9.6.21}$$

where $\overline{f}$ is the *mean force* and A_{ij} is the *force–fabric tensor* given by the expressions

$$\overline{f} = \frac{1}{4\pi}\int_0^{2\pi}\int_0^{\pi} f_n \sin\phi \, \mathrm{d}\phi \, \mathrm{d}\theta \tag{9.6.22}$$

$$\boldsymbol{A} = \begin{bmatrix} 1+a_n & 0 & 0 \\ 0 & 1-a_n/2+3b_n & 0 \\ 0 & 0 & 1-a_n/2-3b_n \end{bmatrix} \tag{9.6.23}$$

and the constants a_n, b_n, a_s, and a_t defined the force–fabric distribution.

For this type of granular material modeling, the Cauchy stress is commonly expressed as an average outer or dyadic product of the branch vectors with the particle contact force

$$T_{ij} = = \frac{1}{N^c}\sum_{v} l_i^c f_j^c \tag{9.6.24}$$

For spherical particles, we assume an average branch vector length $\overline{l}$, and incorporating the previous relations, we can express (9.6.24) as

$$T_{ij} = A_{pq} D_{mn} T_{ijpqmn} \tag{9.6.25}$$

where

$$T_{ijpqmn} = m_v \overline{l}\ \overline{f}\int_0^{2\pi}\int_0^{\pi} (n_p n_q n_i n_j + a_s n_p s_q s_i n_j + a_t n_p t_q t_i n_j) n_m n_n \sin\phi \, \mathrm{d}\phi \, \mathrm{d}\theta \tag{9.6.26}$$

where m_v is the total number of contacts per unit volume (RVE). Under the stated modeling assumptions, relations (9.6.25) and (9.6.26) then give a constitutive relationship between the stress and material and force fabric. Chang and Liu (2013) conducted numerical discrete element modeling for some biaxial and triaxial test configurations and found good agreement with this fabric modeling scheme.

We have presented only a couple of studies that employ continuum mechanics to model the response of granular materials. Many other micromechanical models have been applied to such materials that incorporate fabric in different ways. Some studies have explored plastic and flow response of granular media. This has been an active research field, and because of the complexity of granular materials, this research is expected to continue.

9.7 CONTINUUM DAMAGE MECHANICS

We now wish to explore yet another aspect of micromechanical material behavior which is related to the internal damage within solid media. We assume that this damage initially occurs at length scales several orders of magnitude smaller than that used to analyze the problem. Thus, the damage evolution would be referred to as a micromechanical process. Internal damage identification and characterization is of course very important in the development of safe and reliable materials and structures. Continuum damage mechanics (CDM) is concerned with the macrolevel

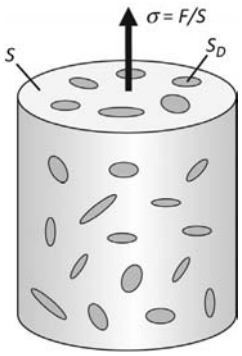

FIGURE 9.19

One-dimensional deformation of damaged material.

characterization and modeling of the effects of distributed defects on the overall material behavior. These defects commonly take the form of microcracks and microcavities, breakage of bonds, collapse of cells and fibers, interfacial decohesions, etc., and these occur in most every material. The goal of CDM is to properly model such discontinuous defects by some type of continuum theory. Due to the statistical nature of material defects, use of an RVE and homogenization methods are often used in developing CDM models.

As usual, our presentation here will only be very brief with just enough information to provide an introduction to the field. This requires that we focus discussion again only on the elastic response. This area of study was initiated in the late 1950s and has now developed into a mature applied science. Major texts including Kachanov (1986), Lemaitre (1996), Krajcinovic (1996), and Voyiadjis and Kattan (2005) as well as review articles such as Chaboche (1988a,b) and Kondo et al. (2007) that provide more details on this topic.

In order to begin our presentation, it will be useful if we first explore the simple one-dimensional uniaxial loading case of a damaged material as illustrated in Fig. 9.19. The material sample (RVE) is assumed to have a distributed collection of damaged zones, and in particular these affect the surface area S by reducing the effective area to be S–S_D as shown, where S_D is the total defect area on the plane under study. We then can define a *surface damage variable* D as

$$D = \frac{S_D}{S} \tag{9.7.1}$$

Note that the damage parameter is bounded by $0 \le D \le 1$, where $D = 0$ corresponds to the undamaged case, while $D = 1$ represents the fully damaged material. Using this simple concept, the standard uniaxial stress expression $\sigma = F / S$ is therefore modified to

$$\bar{\sigma} = \frac{F}{S - S_D} = \frac{F}{S(1 - S_D / S)} = \frac{\sigma}{1 - D} \tag{9.7.2}$$

where $\bar{\sigma}$ is normally called the *effective stress*. Because we have subtracted out the defect area, this stress is sometimes referred to as acting on a fictitious undamaged material. Each of these stresses are related to the strain by a uniaxial Hooke's law $\sigma = E\varepsilon$ and $\bar{\sigma} = \bar{E}\bar{\varepsilon}$, where E is the modulus of the damaged material and $\bar{E}$ is the modulus of the effective (undamaged) material. Linking these relations is commonly done by using a *strain equivalence principle* whereby it is assumed that the strains in the damaged and undamaged configurations are the same. Thus, we can write

$$\varepsilon = \bar{\varepsilon} \Rightarrow \frac{\sigma}{E} = \frac{\bar{\sigma}}{\bar{E}} \tag{9.7.3}$$

Then combining relations (9.7.2) and (9.7.3) gives the modulus of the damaged material

$$E = (1 - D)\bar{E} \tag{9.7.4}$$

and the modified constitutive relation can thus be expressed as

$$\sigma = (1 - D)\bar{E}\varepsilon \tag{9.7.5}$$

Note that as expected, $E \leq \bar{E}$.

Now in order to use this uniaxial relation (9.7.4), we would need a *damage evolution law* which would predict the functional relationship between the damage parameter D and the strain

$$D = \hat{f}(\varepsilon) \tag{9.7.6}$$

This function could be determined from a standard uniaxial tension test. However, such a form would only be valid for monotonic loading, since during an unloading/reloading phase, we expect the damage parameter would keep its maximum value that had been reached before. A common scheme to handle this unloading/reloading problem is to introduce a variable say κ which corresponds to the maximum level of strain reached in the material before current time t:

$$\kappa(t) = \max \varepsilon(\tau), \quad \tau \leq t \tag{9.7.7}$$

Thus, we can then rewrite (9.7.6) as

$$D = \hat{f}(\kappa) \tag{9.7.8}$$

which is now valid for all load histories.

It is often convenient to introduce a *limit state function* as the difference between the strain and its previous maximum value

$$f(\varepsilon, \kappa) = \varepsilon - \kappa \tag{9.7.9}$$

Then the following conditions are often connected with relation (9.7.9):

$$f \leq 0, \quad \dot{\kappa} \geq 0, \quad \dot{\kappa} f = 0 \tag{9.7.10}$$

The first condition implies that the strain ε can never be greater than κ and the second condition indicates that κ cannot decrease.

Using this uniaxial theory, we can examine a typical elastic stress–strain curve for a damaging material as shown in Fig. 9.20. We note that the stress–strain law (9.7.5) is of classical form with a secant modulus $E_s = E = (1-D)\bar{E}$ associated with the damaged material. The material response becomes nonlinear because of the damage, but unloading is done in a linear fashion with modulus E_s.

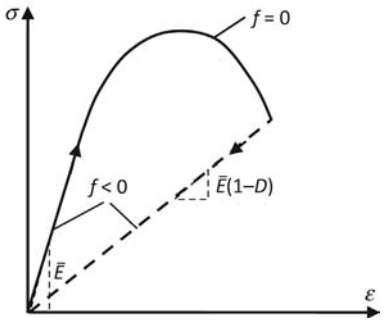

FIGURE 9.20

Uniaxial elastic stress–strain response of a damaged material during loading–unloading.

EXAMPLE 9.7.1 NUMERICAL EVALUATION AND PLOT OF UNIAXIAL DAMAGE MODEL

Using the previous uniaxial continuum damage model with a damage evolution relation $D = \hat{f}(\varepsilon) = 1 - e^{-m\varepsilon}$ (m = constant), calculate and plot the damage evolution and stress–strain response for a monotonic loading situation.

Solution: The MATLAB code for this example is easily constructed; see code C-25 in Appendix C. The code makes two plots: damage parameter evolution with strain, and the stress–strain results for the cases m = 0.5, 1.0, 1.5. These results are shown in Fig. 9.21. It is clearly demonstrated that as the damage parameter increases, the stress response is significantly reduced. This result is of course the expected behavior.

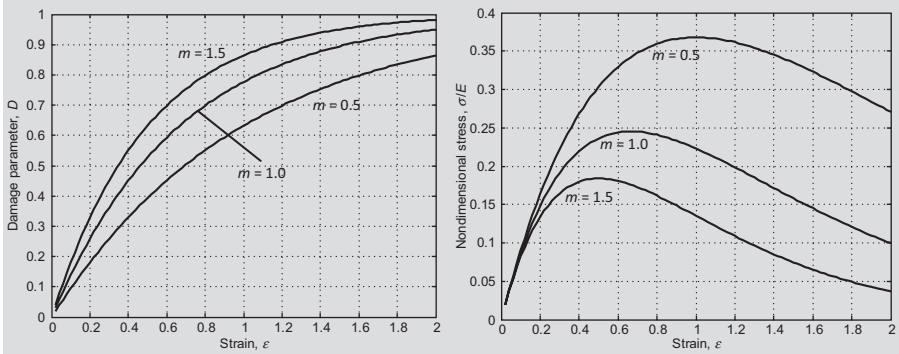

FIGURE 9.21

Numerical results for uniaxial damage model with $D = \hat{f}(\varepsilon) = 1 - e^{-m\varepsilon}$.

We can extend this simple uniaxial model to a three-dimensional elastic case where the elasticity tensor C_{ijkl} for the damaged material can be expressed in terms of the undamaged material tensor C^{o}_{ijkl} as

$$C_{ijkl} = (1-D)C^{o}_{ijkl} \tag{9.7.11}$$

and thus the constitutive relation becomes

$$T_{ij} = (1-D)C^{o}_{ijkl}\varepsilon_{kl} \tag{9.7.12}$$

The corresponding effective stress is then given through the usual equation

$$T_{ij} = (1-D)\bar{T}_{ij} \tag{9.7.13}$$

Now for the three-dimensional case, the damage evolution relation (9.7.9) can be generalized to

$$f(\boldsymbol{\varepsilon}, \kappa) = \varepsilon_{eq}(\boldsymbol{\varepsilon}) - \kappa \tag{9.7.14}$$

where the equivalent strain could be chosen as

$$\varepsilon_{eq}(\boldsymbol{\varepsilon}) = \sqrt{\varepsilon_{ij}\varepsilon_{ij}} \tag{9.7.15}$$

or another choice sometimes proposed is based on the elastic strain energy

$$\varepsilon_{eq}(\boldsymbol{\varepsilon}) = \sqrt{C^{o}_{ijkl}\varepsilon_{ij}\varepsilon_{kl}} \tag{9.7.16}$$

Note that using the simple scalar product approach used in form (9.7.11) places the damage parameter equally on all elastic moduli C^{o}_{ijkl}. This approach is generally referred to as *isotropic damage theory* and would likely have difficulty predicting behaviors for anisotropic materials.

Often CDM theory is generated from thermodynamic principles of irreversible processes. Following similar formulations as used in Sections 7.2 and 7.4, we can start with an appropriate definition of the free energy in terms of the strain and the damage parameter D:

$$\Psi = \Psi(\boldsymbol{\varepsilon}, D) = \frac{1}{2\rho}(1-D)C^{o}_{ijkl}\varepsilon_{ij}\varepsilon_{kl} \tag{9.7.17}$$

where ρ is the mass density, and we have used the usual strain equivalency principle. The stress is then given by

$$T_{ij} = \rho\frac{\partial \Psi}{\partial \varepsilon_{ij}} = (1-D)C^{o}_{ijkl}\varepsilon_{kl} \tag{9.7.18}$$

which is the same as Eq. (9.7.12).

For the isotropic case, we can express the strain in terms of the stress as

$$\varepsilon_{ij} = \frac{1+\nu}{E}\frac{T_{ij}}{(1-D)} - \frac{\nu}{E}\frac{T_{kk}}{(1-D)}\delta_{ij} \tag{9.7.19}$$

It is noted from this constitutive form that only the modulus of elasticity is affected ($\bar{E} = (1-D)E$) by the damage theory and Poisson's ratio remains the same.

Next, we consider another thermodynamic potential

$$Y = -\rho \frac{\partial \Psi}{\partial D} = \frac{1}{2} C^{\circ}_{ijkl} \varepsilon_{ij} \varepsilon_{kl} \tag{9.7.20}$$

which is referred to as the *damage energy release rate*. Using relation (9.7.17), we can express Y in terms of the elastic strain energy $U = \frac{1}{2} C_{ijkl} \varepsilon_{ij} \varepsilon_{kl}$ as

$$Y = \frac{U}{1-D} \tag{9.7.21}$$

Next, consider the case at *constant stress* which implies

$$dT_{ij} = C^{\circ}_{ijkl} [(1-D)\, d\varepsilon_{kl} - \varepsilon_{kl}\, dD] = 0 \Rightarrow d\varepsilon_{kl} = \frac{dD}{1-D} \varepsilon_{kl} \tag{9.7.22}$$

For this case, the elastic strain energy is given by

$$\begin{aligned} dU &= T_{ij}\, d\varepsilon_{ij} = T_{ij} \varepsilon_{ij} \frac{dD}{1-D} \\ &= (1-D) C^{\circ}_{ijkl} \varepsilon_{kl} \varepsilon_{ij} \frac{dD}{1-D} \\ &= C^{\circ}_{ijkl} \varepsilon_{ij} \varepsilon_{kl}\, dD \end{aligned} \tag{9.7.23}$$

and thus

$$\begin{aligned} &\left. \frac{dU}{dD} \right|_{T=\text{const.}} = C^{\circ}_{ijkl} \varepsilon_{ij} \varepsilon_{kl} = 2Y \Rightarrow \\ &Y = \frac{1}{2} \left. \frac{dU}{dD} \right|_{T=\text{const.}} \end{aligned} \tag{9.7.24}$$

For the elastic case, this implies that Y is the strain energy release rate through loss of stiffness which occurs due to damage.

It is sometimes useful to express the general form (9.7.21) for the damage energy release rate in terms of the hydrostatic and effective (von Mises) stresses. Using the results from Section 4.5, we decompose the stress tensor into spherical and deviatoric parts and also use the definition of the effective stress σ_e:

$$\begin{aligned} T_{ij} &= \sigma_H \delta_{ij} + \hat{T}_{ij} \\ \sigma_e &= \sqrt{\frac{3}{2} \hat{T}_{ij} \hat{T}_{ij}} \end{aligned} \tag{9.7.25}$$

where the hydrostatic stress is given by $\sigma_H = \frac{1}{3} T_{kk}$. Using these results, relation (9.7.21) can be expressed as

$$Y = \frac{U}{1-D} = \frac{\sigma_e^2}{2\bar{E}(1-D)^2} \left[\frac{2}{3}(1+\nu) + 3(1-2\nu) \left(\frac{\sigma_H}{\sigma_e} \right)^2 \right] \tag{9.7.26}$$

The ratio $\left(\frac{\sigma_H}{\sigma_e}\right)$ is referred to as the *triaxiality ratio* and it plays a role in the rupture of materials.

Because of the limitations of using only a scalar damage parameter, more general theories have been developed which incorporate a *damage tensor model*. Following the concept first shown in relation (9.7.13), we can express the effective stress relation in a more general scheme

$$\bar{T}_{ij} = M_{ijkl} T_{kl} \tag{9.7.27}$$

where M_{ijkl} is a *fourth-order damage effect tensor*. If $\boldsymbol{M}$ is left to be completely general, the effective stress could become nonsymmetric. This situation is normally avoided. Several different forms of $\boldsymbol{M}$ have been proposed in the literature, and often these have expressed the fourth-order tensor in terms of a second-order damage tensor. This scheme makes it easier to characterize with material parameters. One such form provided by Voyiadjis and Kattan (2005) is

$$M_{ijkl} = (\delta_{ik} - \phi_{ik})^{-1/2} (\delta_{jl} - \phi_{jl})^{-1/2} \tag{9.7.28}$$

where ϕ_{ij} is a *second-order damage tensor*. Further details on this and other types of tensor formulations can be found in the quoted references.

We have only presented a brief outline of CDM that illustrates how continuum mechanics plays an important role in the formulation. Many additional details on damage evolution through physical behaviors including fracture mechanics, dislocation motions, fatigue, plasticity, creep, etc. are commonly incorporated into the theory. This material is well beyond the scope of the text and can be found in the quoted literature.

REFERENCES

Aifantis, E.C., 2003. Update on a class of gradient theories. Mech. Mater. 35, 259–280.

Askes, H., Aifantis, E.C., 2011. Gradient elasticity in statics and dynamics: an overview of formulations, length scale identification procedures, finite element implementations and new results. Int. J. Solids Struct. 48, 1962–1990.

Boresi, A.P., Chong, K.P., 2000. Elasticity in Engineering Mechanics. John Wiley, New York.

Carlson, D.E., 1966. Stress functions for plane problems with couple stresses. J. Appl. Math. Phys. 17, 789–792.

Chaboche, J.L., 1988a. Continuum damage mechanics: Part I. General concepts. J. Appl. Mech. 55, 59–64.

Chaboche, J.L., 1988b. Continuum damage mechanics: Part II. Damage growth, crack initiation, and crack growth. J. Appl. Mech. 55, 65–72.

Chang, C.S., Liu, Y., 2013. Stress Fabric Granular Mater. 2.

Chang, C.S., Ma, L.A., 1991. Micromechanical-base micro-polar theory for deformation of granular solids. Int. J. Solids Struct. 28, 67–86.

Charalambakis, N., 2010. Homogenization techniques and micromechanics. A survey and perspectives. Appl. Mech. Rev. 63.

Chen, K.C., Lan, J.Y., 2008. Microcontinuum derivation of Goodman-Cowin theory for granular materials. Con. Mech. Thermodyn. 20, 331–345.
Cowin, S.C., Nunziato, J.W., 1983. Linear elastic materials with voids. J. Elasticity 13, 125–147.
Cowin, S.C., Puri, P., 1983. The classical pressure vessel problems for linear elastic materials with voids. J. Elasticity 13, 157–163.
Cowin, S.C., 1984a. A note on the problem of pure bending for a linear elastic material with voids. J. Elasticity 14, 227.
Cowin, S.C., 1984b. The stresses around a hole in a linear elastic material with voids. Q. J. Mech. Appl. Math. 37, 441–465.
Cowin, S.C., 1985a. The viscoelastic behavior of linear elastic materials with voids. J. Elasticity 15, 185–191.
Cowin, S.C., 1985b. The relationship between the elasticity tensor and the fabric tensor. Mech. Matl. 4, 137–147.
Cundall, P.A., Strack, O.D., 1979. A discrete numerical model for granular assemblies. Geotchnique 29, 47–65.
Ellis, R.W., Smith, C.W., 1967. A thin-plate analysis and experimental evaluation of couple-stress effects. Exp. Mech. 7, 372–380.
Eringen, A.C., 1968. Theory of micropolar elasticity. Liebowitz, H. (Ed.), Fracture, 2, Academic Press, New York, pp. 662–729.
Eringen, A.C., 1972. Linear theory of nonlocal elasticity and dispersion of plane waves. Int. J. Eng. Sci. 10, 425–435.
Eringen, A.C., 1977. Edge dislocation in nonlocal elasticity. Int. J. Eng. Sci. 15, 177–183.
Eringen, A.C., 1983. On differential equations of nonlocal elasticity and solution of screw dislocation and surface waves. Int. J. Appl. Phys. 54, 4703–4710.
Eringen, A.C., 1999. Microcontinuum Field Theories. I. Foundations and Solids. Springer, New York.
Fang, C., Wang, Y., Hutter, K., 2006. A thermo-mechanical continuum theory with internal length for cohesionless granular materials. Con. Mech. Thermodyn. 17, 545–576.
Ferrari, M., Granik, V.T., Imam, A., Nadeau, J., 1997. Advances in Doublet Mechanics. Springer, Berlin.
Fish, J., Kuznetsov, S., 2012. From homogenization to generalized continua. Intl. J. Comp. Meth. Eng. Mech. 13, 77–87.
Goodman, M.A., Cowin, S.C., 1972. A continuum theory for granular materials. Arch. Rat. Mech. Anal. 44, 249–266.
Granik, V.T., 1978. Microstructural mechanics of granular media. Technique Report IM/MGU 78-.[241]. Inst. Mech. of Moscow State University [in Russian].
Granik, V.T., Ferrari, M., 1993. Microstructural mechanics of granular media. Mech. Mater. 15, 301–322.
Gutkin, M.Y., Aifantis, E.C., 1996. Screw dislocation in gradient elasticity. Scripta Matl. 35, 1353–1358.
Hartranft, R.J., Sih, G.C., 1965. The effect of couple-stress on the stress concentration of a circular inclusion. J. Appl. Mech. 32, 429–431.
Hill, R., 1963. Elastic properties of reinforced solids: some theoretical principles. J. Mech. Phys. Solids 11, 357–372.
Kachanov, L.M., 1986. Introduction to Continuum Damage Mechanics. Springer, Dordrecht, the Netherlands.
Kaloni, P.N., Ariman, T., 1967. Stress concentration effects in micropolar elasticity. J. Appl. Math. Phys. 18, 136–141.

Kennedy, T.C., Kim, J.B., 1987. Finite element analysis of a crack in a micropolar elastic material. Raghavan, R., CoKonis, T.J. (Eds.), Computers in Engineering, 3, ASME, pp. 439–444.
Kennedy, T.C., 1999. Modeling failure in notched plates with micropolar strain softening. Composite Struct. 44, 71–79.
Kondo, D., Welemane, H., Cormery, F., 2007. Basic concepts and models in continuum damage mechanics. Rev. Eur. Genie 11, 927–943.
Krajcinovic, D., 1996. Damage Mechanics. North-Holland, Amsterdam.
Kunin, I.A., 1983. Elastic Media with Microstructure. II. Three-Dimensional Models. Springer, Berlin.
Lazar, M., Maugin, G.A., 2006. A note of line forces in gradient elasticity. Mech. Res. Commun. 33, 674–680.
Lemaitre, J., 1996. A Course on Damage Mechanics. Springer, Berlin.
Li, S., Miskioglu, I., Altan, B.S., 2004. Solution to line loading of a semi-infinite solid in gradient elasticity. Int. J. Solid Struct. 41, 3395–3410.
Li, X., Yu, H.S., Li, X.S., 2009. Macro-micro relations in granular mechanics. Int. J. Solids Struct. 46, 4331–4341.
Mehrabadi, M.M., Nemat-Nasser, S., Oda, M., 1982. On statistical description of stress and fabric in granular materials. Int. J. Num. Anal. Meth. Geomech. 6, 95–108.
Mindlin, R.D., 1963. Influence of couple-stress on stress concentrations. Exp. Mech. 3, 1–7.
Mindlin, R.D., 1964. Microstructure in linear elasticity. Arch. Rat. Mech. Anal. 16, 51–78.
Mindlin, R.D., 1965. Second gradient of strain and surface tension in linear elasticity. Int. J. Solids Struct. 1, 417–438.
Nemat-Nasser, S., Hori, H., 1993. Micromechanics: overall properties of heterogeneous materials. Applied Mathematics and Mechanics Series, Vol 37. North-Holland, Amsterdam.
Nguyen, V.P., Stroeven, M., Sluys, L.J., 2011. Multiscale continuous and discontinuous modeling of heterogeneous materials: a review on recent developments. J. Multiscale Model. 3, 1–42.
Nicot, F., Darve, F., 2005. A multi-scale approach to granular materials. Mech. Mater. 37, 980–986.
Nowacki, W., 1986. Theory of Asymmetric Elasticity. Pergamon Press, Oxford.
Ru, C.Q., Aifantis, E.C., 1993. A simple approach to solve boundary-value problems in gradient elasticity. Acta Mech. 101, 59–68.
Sadd, M.H., 2014. Elasticity: Theory, Applications and Numerics, Third ed Elsevier, Waltham, MA.
Sadd, M.H., Dai, Q., 2004. A comparison of micromechanical modeling of asphalt materials using finite elements and doublet mechanics. Mech. Mater. 37, 641–662.
Sadd, M.H., Dai, Q., Parmameswaran, Shukla, A., 2004. Microstructural simulation of asphalt materials: modeling and experimental studies. J. Mater. Civil Eng. 16, 107–115.
Sadd, M.H., Qiu, L., Boardman, W.G., Shukla, A., 1992. Modelling wave propagation in granular media using elastic networks. Int. J. Rock Mech. Min. Sci. Geomech. 29, 161–170.
Schijve, J., 1966. Note of couple stresses. J. Mech. Phys. Solids 14, 113–120.
Sun, C.T., Yang, T.Y., 1975. A couple-stress theory for gridwork-reinforced media. J. Elasticity 5, 45–58.
Toupin, R.A., 1964. Theories of elasticity with couple-stress. Arch. Rat. Mech. Anal. 17, 85–112.
Weitsman, Y., 1965. Couple-stress effects on stress concentration around a cylindrical inclusion in a field of uniaxial tension. J. Appl. Mech. 32, 424–428.
Voyiadjis, G.Z., Kattan, P.I., 2005. Damage Mechanics. Taylor & Francis, Boca Raton, FL.

EXERCISES

9.1 Verify the two-dimensional couple-stress constitutive relations (9.2.10).

9.2 Justify the compatibility equations (9.2.12).

9.3 Verify that the two-dimensional stress–stress function relations (9.2.14) are a self-equilibrated form.

9.4 For the couple-stress theory, show that the two stress functions satisfy

$$\nabla^4\Phi = 0, \quad \nabla^2\Psi - l^2\nabla^4\Psi = 0$$

9.5 Using the general stress relations (9.2.25) for the stress concentration problem of Example 9.2.1, show that the circumferential stress on the boundary of the hole is given by

$$T_{\theta\theta}(a,\theta) = T\left(1 - \frac{2\cos 2\theta}{1+F}\right)$$

Verify that this expression gives a maximum at $\theta = \pm\pi/2$, and explicitly show that this value will reduce to the classical case of $3\boldsymbol{T}$ by choosing $l_1 = l_2 = l = 0$.

9.6 For isotropic couple-stress theory, it has been proposed to use a hyperelastic formulation such that the strain energy function may be specified by

$$U = \frac{1}{2}\lambda\varepsilon_{kk}\varepsilon_{mm} + \mu(\varepsilon_{km}\varepsilon_{km} + l^2\chi_{km}\chi_{km})$$

where λ and μ are the usual elastic constants, ε_{ij} is the strain tensor, l^2 is a length parameter, and χ_{ij} is the *symmetric curvature tensor* defined by $\chi_{ij} = \frac{1}{2}(\omega_{i,j} + \omega_{j,i})$ with the rotation vector given by $\omega_i = \frac{1}{2}\varepsilon_{ijk}u_{k,j}$. Using the relations $T_{ij} = \frac{\partial U}{\partial \varepsilon_{ij}}$ and $m_{ij} = \frac{\partial U}{\partial \chi_{ij}}$, show that the constitutive relations for the stress and couple-stress are given by

$$T_{ij} = \lambda\varepsilon_{kk}\delta_{ij} + 2\mu\varepsilon_{ij}, \quad m_{ij} = 2\mu l^2\chi_{ij}$$

9.7 For the formulation given in Exercise 9.6, consider a torsional displacement field $u_1 = 0, u_2 = -\kappa x_1 x_3, u_3 = \kappa x_1 x_2$, where κ is a constant. Determine the strains, rotations, symmetric curvature tensor, and then using the constitutive relations calculate the stresses and couple-stresses.

9.8 Starting with the general relations (9.3.6), verify that the two-dimensional plane stress constitutive equations for elastic materials with voids are given by (9.3.9).

9.9 For elastic materials with voids, using the usual single strain compatibility equation, develop the stress and stress-function compatibility forms (9.3.10) and (9.3.11).

9.10 Using the inequalities (9.3.7), verify that the length parameter h^2 defined by relation (9.3.13) is positive.

9.11 Compare the hoop stress $T_{\theta\theta}(r, \pi/2)$ predictions from elasticity with voids given by relation (9.3.18) with the corresponding results from classical theory. Choosing $N = 1/2$ and $L = 2$, for the elastic material with voids, make a comparative plot of $T_{\theta\theta}(r, \pi/2)/T$ versus r/a for these two theories.

9.12 Verify the doublet mechanics $\boldsymbol{Q}$ transformational matrix given by relation (9.4.10) in Example 9.4.1.

9.13 For the doublet mechanics Flamant solution in Example 9.4.1, develop contour plots (similar to Fig. 9.10) for the microstresses p_1 and p_2. Are there zones where these microstresses are tensile?

9.14 Consider the gradient elasticity problem under a one-dimensional deformation field of the form $u = u(x), v = w = 0$. Using constitutive form (9.5.3), determine the stress components. Next show that equilibrium equations reduce to $\dfrac{dT_x}{dx} = 0$, and this will lead to the equation

$$\frac{d^4u}{dx^4} - \frac{1}{c}\frac{d^2u}{dx^2} = 0$$

Finally show that the solution for the displacement is given by

$$u = c_1 + c_2 x + c_3 \sinh\left(\frac{x}{\sqrt{c}}\right) + c_4 \cosh\left(\frac{x}{\sqrt{c}}\right)$$

9.15 Starting with the given displacement form (9.5.10), explicitly justify relations (9.5.11)–(9.5.14) in the gradient dislocation Example 9.5.1.

9.16 Using integral tables verify that the gradient Flamant stress integral solution reduces to the classical elasticity form as per Eq. (9.5.22).

9.17 Justify the reduced fabric constitutive form (9.6.6).

9.18 For the isotropic fabric tensor case $M_{ij} = M_o \delta_{ij}$, explicitly justify relations (9.6.10)–(9.6.12).

9.19 Consider the case of a fabric tensor given by

$$M_{ij} = \begin{bmatrix} M_1 & 0 & 0 \\ 0 & M_2 & 0 \\ 0 & 0 & M_3 \end{bmatrix}$$

Using relation (9.6.8), determine the components of the elasticity tensor and show that there will be only nine nonzero terms, thus leading to an orthotropic constitutive form.

9.20 Consider the two-dimensional fabric tensor formulation in Section 9.6. Using the distribution function $\xi(\phi) = \dfrac{1}{2\pi}(1 + a\cos 2\phi)$, first show that

it satisfies the probability relation $\int_0^{2\pi} \xi(\phi)\, d\phi = 1$. Next noting that the normal vector is now given by $\boldsymbol{n} = (\cos\phi, \sin\phi)$, and $\xi(\boldsymbol{n}) = \dfrac{1}{2\pi} D_{ij} n_i n_j$, $M_{ij} = \int_0^{2\pi} \xi(\phi) n_i n_j \, d\phi$, verify that the contact density and fabric tensors are given by $\boldsymbol{D} = \begin{bmatrix} 1+a & 0 \\ 0 & 1-a \end{bmatrix}, \boldsymbol{M} = \dfrac{1}{2}\begin{bmatrix} 1+a/2 & 0 \\ 0 & 1-a/2 \end{bmatrix}$.

9.21 An elastic damage model is sometimes generated from the response of a system of N parallel bars as shown. Each bar is assume to have identical length, material stiffness $k = k_i = A_i E_i / l$, and deformation δ. The load deflection response for the ith bar is then given by $P_i = k_i \delta$, and from equilibrium the total load of the entire assembly is $P = \sum_{i=1}^{N} P_i$. The bars are totally elastic and fail by complete rupture with a given rupture strength distribution among the bars. For the case where if n bars fail, show that $P = k(1-D)\delta$, where the damage parameter is given by $D = n/N$ and $K = Nk$. Note how this result has the same form as relation (9.7.5).

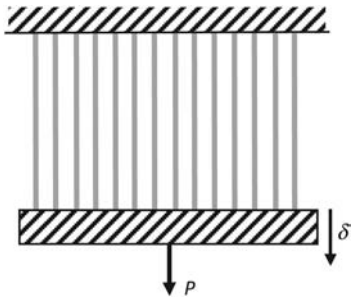

9.22 For uniaxial damage theory, instead of using equivalency of the strain, consider the case of *elastic strain energy equivalency*. For this case, the form of the strain energy is taken to be the same in both the damaged and undamaged (effective) configurations and thus $\dfrac{1}{2}\sigma\varepsilon = \dfrac{\sigma^2}{2E} = \dfrac{\bar{\sigma}^2}{2\bar{E}}$. Show that the new relation for the damaged modulus is given by $E = (1-D)^2 \bar{E}$.

9.23 Similar to Example 9.7.1, consider the uniaxial damage response for the case with a damage evolution relation $D = \hat{f}(\varepsilon) = \dfrac{\varepsilon^2}{m}$ with $0 \le \varepsilon \le 2$ and $m > 4$. Make plots of the damage parameter evolution with strain, and the stress–strain results for the cases $m = 5$, 10, and 20. Note that this case has a smaller damage evolution when compared to the text example.

9.24 Explicitly verify relation (9.7.26) for the damage energy release rate.